NASA/CR—2005–213845

On Structural Design of a Mobile Lunar Habitat With Multi-Layered Environmental Shielding

M. Rais-Rohani
Mississippi State University, Mississippi State, Mississippi

Prepared for Marshall Space Flight Center
under Contract NNM04AA08G
and sponsored by the
NASA Faculty Fellowship Program
managed at the Marshall Space Flight Center

April 2005

The NASA STI Program Office…in Profile

Since its founding, NASA has been dedicated to the advancement of aeronautics and space science. The NASA Scientific and Technical Information (STI) Program Office plays a key part in helping NASA maintain this important role.

The NASA STI Program Office is operated by Langley Research Center, the lead center for NASA's scientific and technical information. The NASA STI Program Office provides access to the NASA STI Database, the largest collection of aeronautical and space science STI in the world. The Program Office is also NASA's institutional mechanism for disseminating the results of its research and development activities. These results are published by NASA in the NASA STI Report Series, which includes the following report types:

- TECHNICAL PUBLICATION. Reports of completed research or a major significant phase of research that present the results of NASA programs and include extensive data or theoretical analysis. Includes compilations of significant scientific and technical data and information deemed to be of continuing reference value. NASA's counterpart of peer-reviewed formal professional papers but has less stringent limitations on manuscript length and extent of graphic presentations.

- TECHNICAL MEMORANDUM. Scientific and technical findings that are preliminary or of specialized interest, e.g., quick release reports, working papers, and bibliographies that contain minimal annotation. Does not contain extensive analysis.

- CONTRACTOR REPORT. Scientific and technical findings by NASA-sponsored contractors and grantees.

- CONFERENCE PUBLICATION. Collected papers from scientific and technical conferences, symposia, seminars, or other meetings sponsored or cosponsored by NASA.

- SPECIAL PUBLICATION. Scientific, technical, or historical information from NASA programs, projects, and mission, often concerned with subjects having substantial public interest.

- TECHNICAL TRANSLATION. English-language translations of foreign scientific and technical material pertinent to NASA's mission.

Specialized services that complement the STI Program Office's diverse offerings include creating custom thesauri, building customized databases, organizing and publishing research results…even providing videos.

For more information about the NASA STI Program Office, see the following:

- Access the NASA STI Program Home Page at ***http://www.sti.nasa.gov***

- E-mail your question via the Internet to help@sti.nasa.gov

- Fax your question to the NASA Access Help Desk at 301–621–0134

- Telephone the NASA Access Help Desk at 301–621–0390

- Write to:
  NASA Access Help Desk
  NASA Center for AeroSpace Information
  7121 Standard Drive
  Hanover, MD 21076–1320
  301–621–0390

NASA/CR—2005–213845

On Structural Design of a Mobile Lunar Habitat With Multi-Layered Environmental Shielding

M. Rais-Rohani
Mississippi State University, Mississippi State, Mississippi

Prepared for Marshall Space Flight Center
under Contract NNM04AA08G
and sponsored by the
NASA Faculty Fellowship Program
managed at the Marshall Space Flight Center

National Aeronautics and
Space Administration

Marshall Space Flight Center • MSFC, Alabama 35812

April 2005

Acknowledgments

This research was conducted in summer of 2004 at the Advanced Projects Office (FD02) of the Flight Projects Directorate at the NASA Marshall Space Flight Center (MSFC), in Huntsville, AL. Funding was provided by the NASA Faculty Fellowship Program and Mississippi State University. The author wishes to thank David Smitherman, Jr. and Joe Howell of SP20 for their sponsorship of this research activity. Daniel Dunn is thanked for his development of solid models for the MLH design concept. Moreover, Jeff Anderson, Ramona Cummings, Jennifer Robinson, Ben Hayashida, Rod Stallworth, Heather Lewis, Tom Delay, Margaret Bruce, Katherine Harine, Richard Altstatt, Manojeet Bhattacharya, John Watts, Jr., Mark Gerry, Clara Welch, and Wayne Parks are thanked for offering helpful suggestions on various topics during the course of this research. A special gratitude goes to Scott Taylor of Morgan Research Corp. for his development of the FE model of MLH based on separate models of the ISS US module and Node 1 graciously provided by the Boeing Co. with the kind assistance of Steven Woletz and Tom Helsper.

Available from:

NASA Center for AeroSpace Information
7121 Standard Drive
Hanover, MD 21076–1320
301–621–0390

National Technical Information Service
5285 Port Royal Road
Springfield, VA 22161
703–487–4650

TABLE OF CONTENTS

LIST OF FIGURES

LIST OF TABLES

CONTRACTOR REPORT

ON STRUCTURAL DESIGN OF A MOBILE LUNAR HABITAT WITH MULTI-LAYERED ENVIRONMENTAL SHIELDING

1. INTRODUCTION

The space exploration science and technology efforts of the past several decades were significantly energized by the recent presidential announcement articulating a new "Vision for Space Exploration", which calls for human lunar return by as early as 2015 and no later than 2020.

The future human lunar missions are expected to undertake far more ambitious activities than those of the Apollo program with the possibility of some missions lasting up to several months. Such extended missions require the use of large-size lunar outposts to accommodate living quarters for the astronauts as well as indoor laboratory facilities.

The greatest obstacle to the prolonged human presence on the Moon is the threat posed by the harsh lunar environment that is plagued with multi-source high-energy radiation exposure as well as frequent barrage of meteoroids. Hence, for such extended missions to succeed, it is vital that the future lunar outposts and the larger-size bases be designed to provide a safe habitat for the astronauts.

Over the past few years, a variety of ideas and concepts for future lunar outposts and bases have been proposed. With shielding as the primary concern, some have suggested the use of natural structures such as lava tubes[1] while others have taken a more industrial approach and suggested the construction of fixed structures in the form of inflatable[2], inflatable with rigid elements[3], erectable[4,5], tent-style membrane[6], and textile filled with regolith[7,8]. For evaluation of these structural design concepts, Drake and Richter[9] have proposed a rating system based on such factors as effectiveness, importance, and timing. While all of these designs, in general, benefit from in-situ resource utilization (i.e., lunar regolith) for shielding, they share a common disadvantage of being fixed to one particular location that would limit exploration to the region in close proximity of the outpost.

As an alternative to the fixed-base concepts, some have suggested mobile lunar outposts (reminiscing of recreational vehicles). While providing a self-contained habitat, such mobile units can offer the future lunar explorers and workers the freedom to travel from one location to another, and to enhance the exploration and scientific activities on the Moon. At the forefront of such concepts is the notional architecture of HARMONY (Human And Robotic MOdular

iNfrastructures/sYstems) proposed by Mankins.[10] As part of his HARMONY architecture, Mankins suggests the use of Modular Integrated Lunar Outpost (MILO) with each module representing a blend of habitat and robotics design referred to as a "Hab-Bot". The idea is to launch these Hab-Bots, ahead of astronauts, to a desired spot on the Moon. Operating in the autonomous or remotely operated control mode, these modules will link up together to form a larger integrated outpost. As a mission comes to an end and the crew has departed, these modules will walk to another location and establish a new outpost prior to the arrival of the next group of astronauts and space workers.

Upon comparing various mobile lunar outpost design architectures, Cohen offers a rationale for the Mankins' Hab-Bot based HARMONY concept as the most viable option.[11] While mobility and integratability are the main advantages of the Hab-Bot design, the greatest drawback to this and all other proposed concepts is the need for the habitat wall to provide the necessary environmental shielding. This requirement poses a serious challenge to the design of the structure, and demands the use of innovative solutions.

As part of this research, a Hab-Bot inspired concept for a Mobile Lunar Habitat (MLH) is proposed, which makes use of advanced composite materials to reduce the habitat's mass and to seek a viable solution to the shielding problem. In the remaining portion of this report, the lunar environmental hazards as related to space radiation, meteoroid impact, and thermal fluctuations, as well as options on how to protect the habitat against each threat are discussed. This discussion is followed by presentation of the MLH design concept, its wall design and constituent material system, as well as the proposed methods of construction. Using a finite-element model of the MLH design, a preliminary static analysis is performed using MSC/NASTRAN with internal pressure as the principal load case. The last section of the report provides some recommendations for future work.

2. SHIELDING AGAINST SPACE RADIATION

Unlike the Earth's surface that is protected by a relatively dense atmosphere and the geomagnetic field, the lunar surface is completely deprived of any natural shielding against harmful space radiation. The ambient radiation environment of the lunar surface consists of energetic ionized particles of solar and galactic origins[12]. The primary concern is with the positively charged particles (protons) that can possess far greater penetration power as compared to the negatively charged particles (electrons).

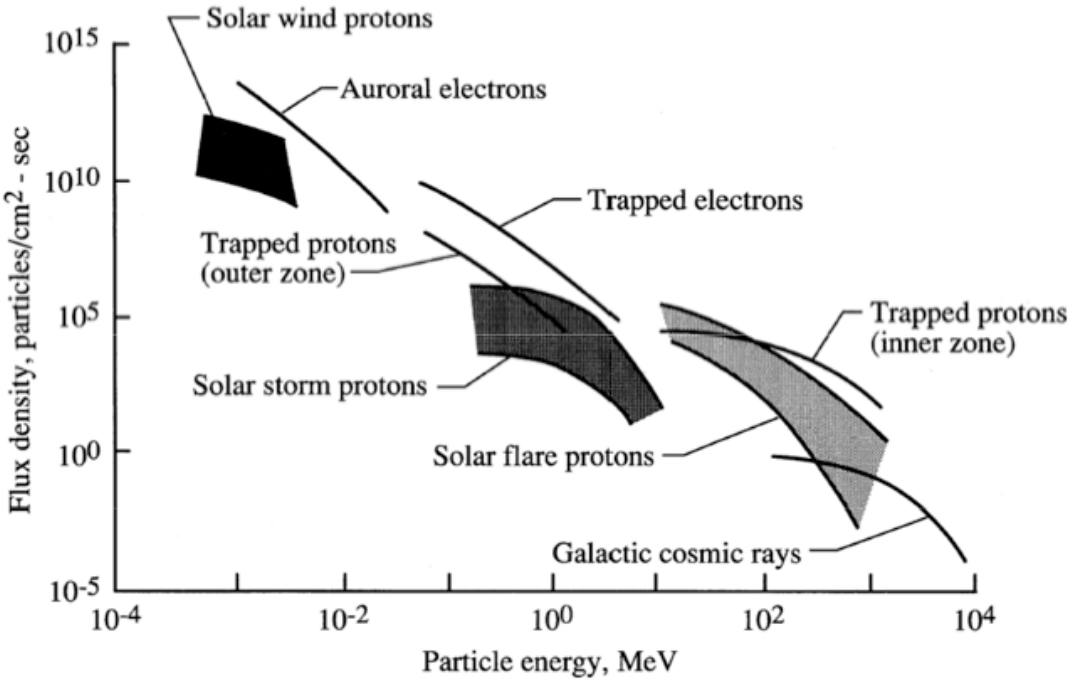

Figure 1: Free-space radiation environment. (figure from Ref. 12)

The Solar Energetic Particles (SEP) are released from the Sun through sporadic flare events, which are correlated with the periods of increased solar activity. The positively charged particles that are released from the Sun mostly consist of hydrogen and helium ions (protons and alpha particles) with a much smaller, but biologically more damaging, heavy-ion component (atomic number, $Z > 2$) that can vary from one event to another.[13] Because the released particles are far more energetic (> 0.1 MeV*), solar flares are of significantly greater concern in shield design than the less energetic but more abundant solar wind and storm particles (see Fig. 1).

The solar flares are short-duration (maximum intensity lasting a day) sporadic events, and are catalogued for each 11-year solar cycle with the year 1997 marking the start of cycle 23. Among the flare events of recent history, those corresponding to February 1956, November 1960, August 1972, and October 1989 are often cited as large flare events that should be considered in

* One electronvolt (eV) is the work required to move an electron through a potential difference of one volt. This unit is used to describe the total energy carried by a particle. 1 eV = 1.602 x 10^{-19} J.

spacecraft and lunar habitat designs[12]. The February 1956 event produced the maximum particle energy of nearly 1 GeV whereas the August 1972 flare produced the greatest number of protons above 10 MeV energy level[12]. Although solar flare events are correlated with periods of active sun, no model has yet been developed to make accurate prediction of individual events[14].

As shown in Fig. 1, the most energetic form of radiation in free-space as well as on the lunar surface is that associated with the nearly constant Galactic Cosmic Rays (GCR), which are believed to have emanated mainly from exploding stars within the Milky Way galaxy. Reaching energies of 10 GeV, GCR particles travel at nearly the speed of light through the very thin gas of interstellar space. At solar minimum conditions, GCR particle fluxes reach their maximum, and conversely reach their minimum at periods of solar maximum. By some estimates, the GCR spectrum, as shown in Fig. 2, consists of approximately 90% hydrogen, 9% helium, and 1% heavier nuclei such as iron (Fe, Z = 26) and nickel (Ni, Z = 28).[15]

Although they constitute the smallest portion of the overall GCR spectrum, the heavy charge and energy (HZE) particles are significantly more potent and biologically damaging than the much more abundant but over fifty times lighter hydrogen ions.

While SEP and GCR particle fluxes at the lunar surface are half as intense as those in the free space (as the Moon shields the space below the horizon), the remaining energized particles can still pose a significant health threat to the astronauts. Furthermore, the direct proton flux streaming from above is also accompanied by the induced neutrons produced at a shallow depth beneath the lunar regolith.

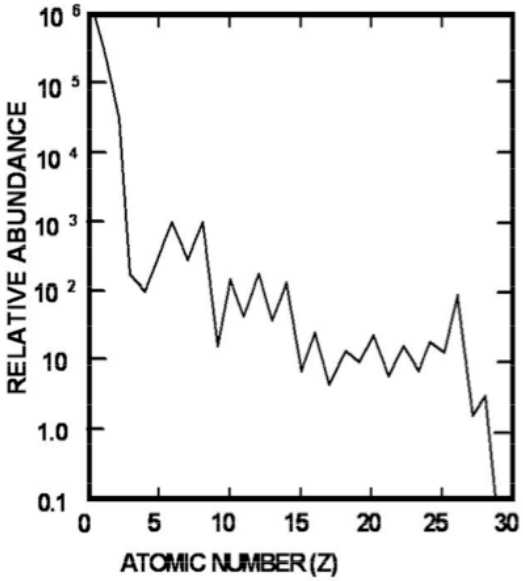

Figure 2: Relative abundance of GCR particles ranging in atomic numbers from 1 to 30. (figure from Ref. 15)

The threat posed by radiation is typically measured in terms of damage it can cause to the cells in the skin (at depth of 0.01 cm), eye (at depth of 0.3 cm), or more importantly the vital blood-forming organs (BFO) (at depth of 5 cm). The depth of 5 cm is adopted for the BFO dose when the detailed body geometry is not considered. The current guidelines for human space activities are those established by NCRP[16], which specifies the radiation exposure limits in low-earth orbit (LEO) to be those as given in Table 1. These limits have been developed with the aim of keeping radiation-induced excess risk of fatal cancer over the astronaut's lifetime to below 3%. Whereas the short-term exposure limits are more critical when considering the high-dose radiation rates associated with solar flare events, the career limits are more applicable for long-term space missions, which are principally affected by GCR radiation.

Measured in SI unit of Sieverts (Sv), the equivalent dose is determined by multiplying the radiation absorbed-dose in Gray (Gy) by the corresponding quality factor as established by the ICRP.[17] The absorbed dose represents the amount of energy deposited per unit of mass.

Table 1: Recommended limits for dose-equivalent radiation exposure in LEO. (from Ref. 16)

Exposure period	BFO, Sv	Eye, Sv	Skin, Sv
30 days	0.25	1.0	1.5
Annual	0.5	2.0	3.0
Career	1.0-4.0[a]	4.0	6.0

[a]Age and gender dependent

Quality factor is unique to the type of incident radiation and has a value of one for linear energy transfer (LET) less than 1 KeV/μm before it begins to sharply increase to its peak value of 30 at LET = 100 KeV/μm, and a rapid drop afterwards[18]. LET is a measurement of the number of ionizations that radiation causes per unit distance as it travels through the cell or biological tissue, and the lateral damage it causes along the path[19]. Whereas medical X-rays are low LET radiation, alpha particles have very high LET. Although the magnitude of human biological effects of exposure to high-LET radiation is not fully understood, the threat of radiation-induced cancers as well as cellular and neurological damage associated with long-duration lunar activities are of great concern.[20] Irreversible biological damage occurs at LET > 10 KeV/μm.

Wilson, et al.[18] state that "*the biological response of living tissues depends (in part) on the temporal and spatial fluctuations of the energy deposits within the tissue system. Such fluctuations depend not only on the specific environment to which the astronaut is exposed but also on how that environment is modified by interaction with the astronaut's body in reaching the specific tissues*."

Without any shielding, an astronaut in free space would receive a BFO dose equivalent of 0.6 Sv/yr from GCR at solar minimum conditions. For the three large solar flare events of August 1972, November 1960, and February 1956, the free-space BFO doses are estimated at 4.11 Sv, 1.10 Sv, and 0.62 Sv, respectively. Clearly the GCR dose is greater than the annual limit whereas the SEP event doses far exceed the 30-day limit as identified in Table 1. For a lunar habitat, in the form of a semi-spherical structure, the dose equivalents would be half the corresponding free-space values. Even then, when considering the SEP events, it is possible to reach or exceed the annual BFO limit in a very short period of time in a poorly shielded environment.[12]

Many factors, such as the material composition and thickness of the habitat wall, the geometry of the habitat, and even the internal equipment and their placements will influence the spatial radiation environment inside the lunar habitat. However, the most crucial factor affecting the overall interior environment is the material composition of the habitat wall. Wilson, et al.[21] cite two important parameters in determining radiation shield effectiveness: 1) stopping the low energy protons by atomic collision, and 2) stopping the production of particles (mostly neutrons) in collision with the shield nuclei. Since it is nearly impossible to engineer a shield that would fully stop the penetration of HZE particles, the ALARA (as low as reasonably achievable) principle has been considered as a guide in the MLH design.

To simulate the transport of energetic particles through various shielding materials along with the induced secondary particles, several particle transport codes such as HZETRN[22], NOVICE[23], and SHIELDOSE-2[24] have been developed.

Numerous studies have been conducted during the past decade on the performance of various materials that either have been used or are being considered for radiation shielding of lunar habitats and spaceships.[25] With the help of HZETRAN code, Wilson and colleagues have compiled annual radiation dose and dose-equivalent estimates for GCR and SEP through slab and spherical shell shields made of aluminum and polyethylene.[26] Their results show that, in general, polyethylene is a far superior shielding material than aluminum. For example, using the maximum observed GCR flux of the 1977 solar minimum at the end of solar cycle 21, the BFO dose equivalent through a shield at areal density (shield thickness) of 5 g/cm^2 is found to be 0.65 Sv/yr for aluminum as compared to 0.58 Sv/yr for polyethylene. However, at the specified thicknesses, the annual BFO limit (see Table 1) would be exceeded by both shielding materials. It is worth noting that the shielding protection increases nonlinearly with an increase in shield thickness.

The supremacy of polyethylene as a radiation shielding material is due to its high hydrogen content (~70%). Hence, the best radiation shield would be one made of liquid hydrogen since it would minimize the production of secondary nuclei, but the engineering design requirements would make it an impractical choice. Water is also considered an excellent shielding material, but not as good as polyethylene.[21]

Townsend et al.[27] developed a plot of BFO dose equivalent in free space versus shield thickness (i.e., areal density) for three different materials as shown in Fig. 3. Without any shielding, the annual dose equivalent from GCR at solar minimum conditions is estimated to be 60 rem/yr or 0.6 Sv/yr. For liquid hydrogen, dose equivalent drops sharply as shield thickness reaches 10 g/cm^2 with further increase in shield thickness resulting in a more gradual reduction in dose equivalent. For water and aluminum shielding, the rate of dose equivalent reduction is high for shielding of about 20 g/cm^2 with more gradual dose reductions afterwards.

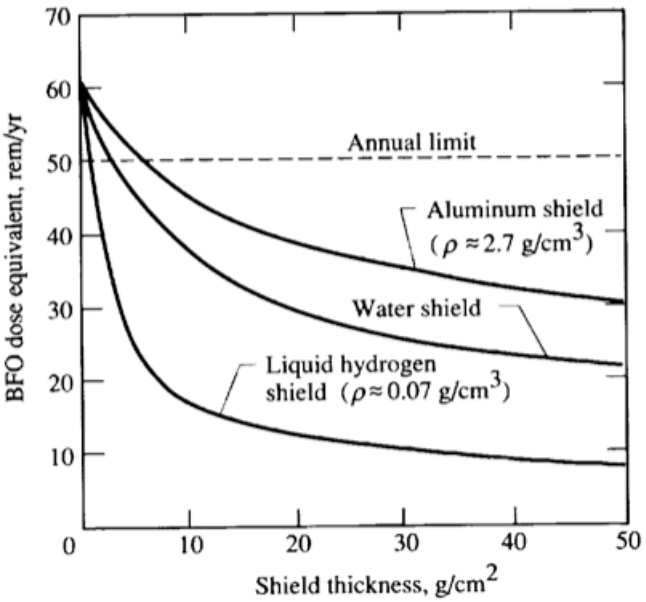

Figure 3: BFO dose equivalent as a function of shield type and thickness resulting from GCR at solar minimum conditions. (figure from Ref. 27)

As noted by Wilson et al.[26], polyethylene at 7 g/cm^2 thickness is considered to provide adequate protection from the combined radiation environment of August 1972 event

and the 1970 GCR. In comparison, the aluminum shield used for the Apollo missions had a thickness of 4.5 g/cm^2.

Although the addition of boron and beryllium to polyethylene is shown to increase the absorption of low-energy (<100 KeV) neutrons[28], Wilson, et al.[21] state that it would be counterproductive for shielding against HZE particles as the increased atomic cross section—caused by the added materials—usually leads to an increased production of secondary neutrons. Fiber-reinforced polymer composite materials are also shown to be good radiation shielding materials as long as the matrix material has a high-hydrogen content.[21]

Several innovative, but technologically more challenging, concepts have also been proposed for radiation shielding. Among them is the active shielding method suggested by Landis.[29] He proposes using magnetic and electrostatic fields to shield against both positively and negatively charged radiation particles. Since the trajectory of charged particles in magnetic field is curved, it is theoretically possible to provide an active shield to change the path of charged particles away from the habitat. However, the technology required for this form of shielding is not yet mature.

Given the technological and logistical challenges of human lunar missions, it may be more practical to design a hybrid system such that passive shielding is used for protection against GCR while active (electromagnetic) shielding is used to boost protection against the sporadic, short-duration SEP events.

3. SHIELDING AGAINST METEOROID IMPACT

Meteoroids originate from both cometary and asteroidal sources. The meteoroid environment near earth and the Moon consists mainly of ice particles of cometary sources. Meteoroids are classified into periodic streams (nearly identical orbits to the source comet) and sporadic (random orbits). The stream meteoroids are caused by the periodic passage of particular comets through the solar system, and are responsible for very localized meteor showers. By contrast, the sporadic meteoroids have a constant presence throughout the year. Although at peak of a shower, the stream meteoroids result in greater fluxes (number of particles per unit area), when integrated over time, the sporadic meteoroids would pose a more significant threat to a spacecraft during an interplanetary space travel and to man-made structures on the lunar surface.

The sporadic meteoroids can hit the lunar surface from different trajectories relative to the ecliptic plane. The meteoroids that travel from the direction of the sun and the opposite direction (i.e., Helion and Antihelion) are associated with short-period comets, most of which belong to the Jupiter family. The Helion and Antihelion sources are centered in the ecliptic plane with a lateral scatter of ± 12º. Rotating 90º from Helion in the ecliptic plane, we encounter the Apex sources ranging from 10º to 40º above and below the ecliptic plane. The Apex sources are associated with long-period comets (period > 200 years). The Toroidal sources are at approximately 90º relative to the ecliptic plane near the north and south poles. It is not clear which comets are responsible for the Toroidal sources.[30]

Besides differences in trajectory, sporadic meteoroids vary in mass and velocity. For meteoroids smaller than 10^{-6} g, Anderson and Smith[31] suggest an average mass density of 2 g/cm^3, 1 g/cm^3 for meteoroids between 10^{-6} and 0.01 g, and 0.5 g/cm^3 for masses above 0.01 g. The uncertainty about the mass of meteoroids is said to be from 0.2 to 5 times the estimated value. This implies an uncertainty of 0.33 to 3 in the estimated flux at a given mass. The plot of interplanetary meteoroid flux as a function of meteoroid size is shown in Fig. 4.

For interplanetary sporadic meteoroids with mass $m < 10$ g and at a distance of one astronomical unit, the cumulative meteoroid flux (number of particle impacts/m^2/yr) against the surface of the Moon or any other object is given as

$$F(m) = c_0\left\{\left(c_1 m^{0.306} + c_2\right)^{-4.38} + c_3\left(m + c_4 m^2 + c_5 m^4\right)^{-0.36} + c_6\left(m + c_7 m^2\right)^{-0.85}\right\} \qquad (1)$$

where $c_0 = 3.156\text{x}10^7$, $c_1 = 2.2\text{x}10^3$, $c_2 = 15$, $c_3 = 1.3\text{x}10^{-9}$, $c_4 = 10^{11}$, $c_5 = 10^{27}$, $c_6 = 1.3\text{x}10^{-16}$, and $c_7 = 10^6$.

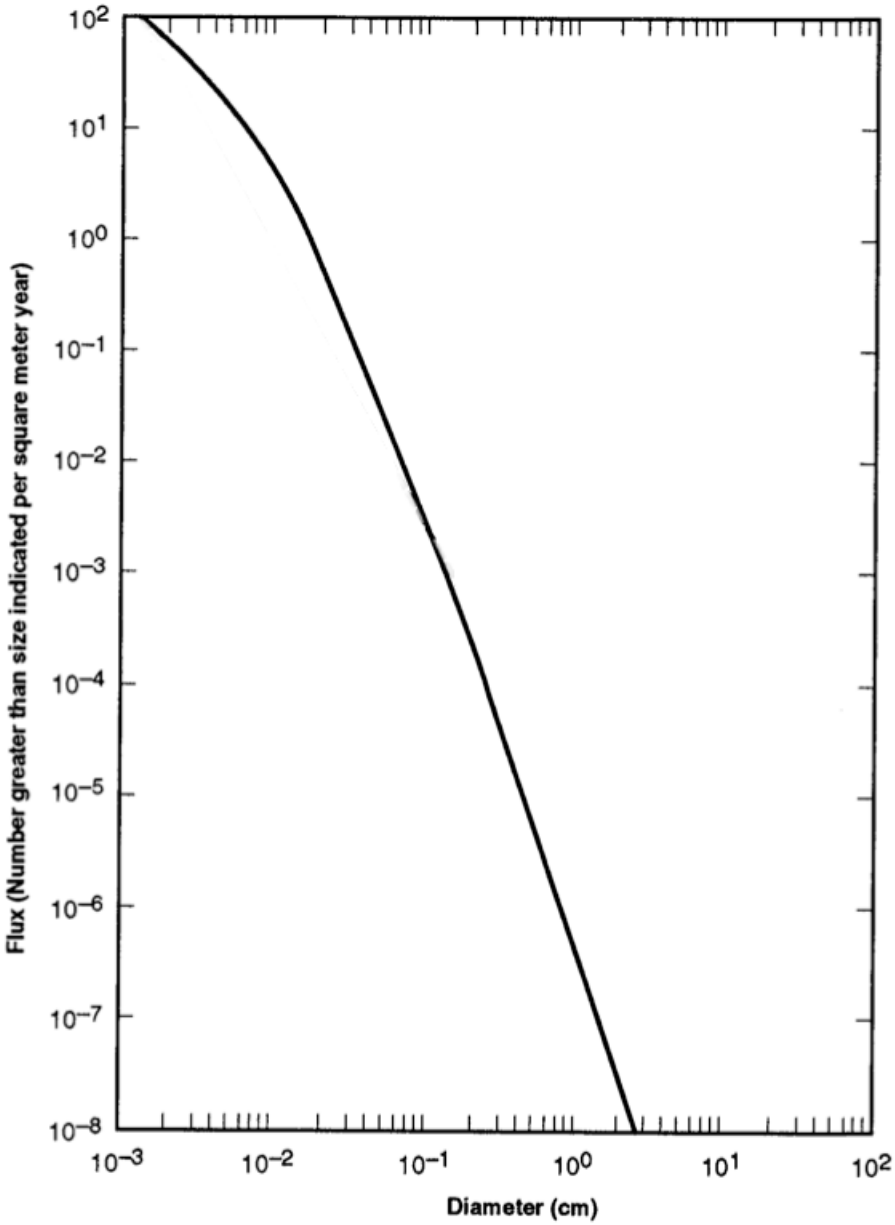

Figure 4: Meteoroid flux as a function of size. (fig. from Ref. 31)

In the interplanetary space, the meteoroids travel at speeds between 11.1 to 72.2 km/s with the number of meteoroids in each speed range (with respect to Earth) given as

$$\begin{aligned} n(V) &= 0.112, && 11.1 \le V < 16.3 \text{ km/s} \\ n(V) &= 3.328\text{x}10^{5} V^{-5.34} && 16.3 \le V < 55 \text{ km/s} \\ n(V) &= 1.695\text{x}10^{-4} && 55 \le V < 72.2 \text{ km/s} \end{aligned} \qquad (2)$$

With the average mass density of 0.5 g/cm^3 and mean speed of approximately 30 km/s, meteoroids and micrometeoroids pose a serious threat to the MLH and the crew working on the lunar surface.

Factors affecting the life times and randomness of sporadic meteoroids in space include viscous-like drag due to Poynting-Robertson (PR) effect, radiation pressure, electromagnetic forces, collision, and gravitational perturbations.[32]

In addition to the meteoroids, lunar ejecta (i.e., particles ejected from the lunar surface as a result of a meteoroid impact) are also of concern.[33] With an estimated mass density of 2.5 g/cm^3 and mean velocity of 0.1 km/s, lunar ejecta can cause damage to MLH, albeit not as bad as the damage that can be caused by a direct meteoroid impact.

Shielding against meteoroid impacts became a major concern with the start of the Apollo program and the expansion of human space activities. The high pressure induced by the hypervelocity meteoroid impact can result in very high strain rates and can cause a serious damage to the shield and whatever is behind it.

In an effort to better understand the hypervelocity impact phenomenon and the potential damage to spacecraft shields, a series of laboratory tests were conducted beginning in the early 1960's. Using primarily single- and two-stage light-gas guns, projectiles of various shape, size, and material were fired at representative samples of spacecraft shields, mostly aluminum. Impact velocity and angle of the projectile along with shield thickness were among the many factors considered. The effect of impact on the shield as well as the projectile were found to depend on many factors, the most important being the impact velocity. Based on the observed test results and analytical studies that followed, projectile impact tests were classified into three phases: ballistic, shatter, and melt/vaporization. A typical curve for projectile diameter versus impact velocity is shown in Fig. 5. Points falling above the curve represent penetration of the shield while those below do not.

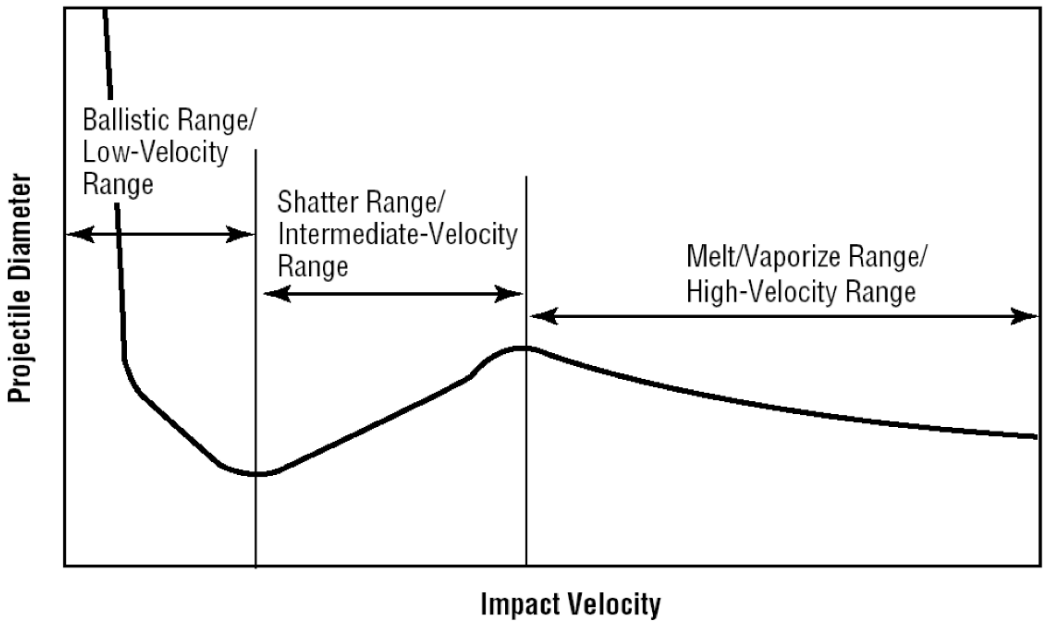

Figure 5: Phase changes in hypervelocity impacts. (figure from Ref. 34)

In low-velocity range, if the projectile penetrates the shield, it will travel along the same path without any significant reduction in speed and without any damage to the projectile. In intermediate-velocity range, if the projectile penetrates the shield, it will shatter and send forth a debris cloud of smaller projectile and shield material particles traveling at slightly dissipated energy level. This behavior is indicated by the upward trend in diameter-velocity curve in Fig. 5. In high-velocity range, the impact energy and the accompanying pressure and temperature are so high that the projectile and the bumper material near the point of impact melt and vaporize.

Based on the results of projectile impact tests, several empirical models for shield damage prediction were developed. One of the first empirical models developed was the Fish and Summers penetration formula given as[33]

$$t_s = K_s m_m^{0.352} V_m^{0.875} \rho_m^{1/6} \tag{3}$$

where t_s is the thickness (cm) of the plate penetrated, K_s represents the combined effects of the shield material's strength, density, ductility, and temperature on threshold penetration, whereas m_m, V_m, and ρ_m represent the mass, velocity, and mass density of the projectile (i.e., the meteoroid), respectively. For 2024-T3 aluminum, stainless steel, and beryllium-copper, K_s is 0.54, 0.32, and 0.30, respectively.[33]

To offer greater protection against meteoroid impact, Whipple suggested placing a thin metal sheet in front of the main shield wall.[35] This "bumper" layer came to be known as the "Whipple Shield", and the resulting double-wall arrangement drastically changed the impact damage characteristics observed in ensuing shield experiments.

Hayashida and Robinson[36,34] have evaluated five analytical penetration models for single-wall and seven models for double-wall configurations made of metallic materials. They compared the accuracy of each model against limited experimental data. The seven models examined for the double-wall configuration were: Original Cour-Palais, Modified Cour-Palais, New Cour-Palais, Nysmith, Lundeberg-Stern-Bristow, Burch, and Wilkinson. All except the Wilkinson's model are based solely on experimental observations from a limited number of projectile tests. Wilkinson's model is derived from linear plate theory and the use of a hydrodynamic computer code to model the response of the rear wall. The Modified and New Cour-Palais equations along with those of Lundeberg-Stern-Bristow and Wilkinson can be used for oblique as well as normal projectile impacts.

In examining three different double-wall shield configurations involving variations in bumper thickness and wall spacing, Hayashida and Robinson[34] show that in the case of low-velocity impact, spacing between the bumper and the rear wall does not have any significant effect. In the intermediate-velocity impact regime, the break-up of projectile into smaller particles dissipates some of the impact energy, and it is found to be less damaging to the rear wall. The bumper spacing, in this case, is seen to have an impact making the double-wall shield design more effective than an equivalent single-plate configuration. As the projectile velocity is increased further, projectile impact results in a cloud of molten/vaporized material with the accompanying shockwave and pressure being more damaging to the rear wall. In this case, the wall spacing is found to have a significant impact in reducing damage to the rear wall. By examining three

combinations of bumper thickness and wall spacing, they found that the double-wall design with a larger spacing (6 in) and thin (0.063 in) bumper thickness outperforms the other two with reduced wall spacing (4 in) at equal or larger (0.08 in) bumper thickness.

It is important to note that all of the analytical models mentioned above were based on experimental results for projectile velocities < 9 km/s. Therefore, there is significant uncertainty about their validity for meteoroids that can travel as fast of 72 km/s. Nonetheless, among the models used in the comparative study[34], the New Cour-Palais equation appears as the most conservative in predicting the impact damage to the bumper and possible penetration of the rear wall.

Gardner et al.[37] developed an analytical equation relating the diameter of the crater or perforation hole to the projectile diameter for impacts in ballistic range at hypervelocities < 15 km/s. They describe the impact phenomenon in metallic plates in terms of projectile diameter and target thickness. For low impact energy, a crater is formed. The crater becomes deeper as the onset of penetration is approached with formation of a lip around the crater. As the projectile diameter exceeds the target thickness, it perforates the target with the resulting hole having similar lips in front and the back. When the projectile diameter becomes an order of magnitude larger than the target thickness, the projectile punches through with minimal difference between the projectile and hole diameters. The analytical equation they developed and validated is given as

$$d_p' = A\left(\frac{10}{9 + e^{D_h'/B}}\right) + D_h'\left(1 - e^{-D_h'/B}\right) \tag{4}$$

where d_p' is the normalized projectile diameter and D_h' the normalized hole diameter with target thickness used as the normalization factor. The parameters A and B are found from curve fitting Eq. (4) to various experimental results. The final forms of A and B are given as

$$A = 6.97\left(\frac{V_p \rho_p}{\sqrt{\sigma_t \rho_t}}\right)^{-0.723}\left(\frac{\sigma_t}{\sigma_{Al}}\right)^{-0.217} t^{-0.053} \tag{5}$$

$$B = B_1 + B_2 V_p \tag{6}$$

where V_p and ρ_p represent the velocity and mass density of the projectile, respectively, whereas σ_t, ρ_t, and t represent the tensile yield strength, mass density, and thickness of the target plate, respectively. The constant terms B_1 and B_2 in Eq. (6) can have a wide range of values and are tabulated by Gardner et al.[37] for different metallic target materials and projectile velocities. In Eq. (5) only the target thickness is measured in μm whereas the other variables can be used in any consistent set of units, SI or otherwise. The maximum target thickness at which penetration can occur (i.e., the ballistic limit) is given as

$$\frac{t_{\max}}{d_p} = 0.129\left(\frac{V_p \rho_p}{\sqrt{\sigma_t \rho_t}}\right)^{0.763}\left(\frac{\sigma_t}{\sigma_{Al}}\right)^{0.229} d_p^{0.056} \qquad (7)$$

Besides the empirical equations discussed above, more rigorous hydrodynamic computer tools are being used to predict the response of shield material to hypervelocity impacts. Two examples of these codes include the commercial code PAM-SHOCK[38], which is currently being tested by the European Space Agency against experimental data for impacts up to 11 km/s, and AUTODYN[39].

With the growing use of nonmetallic composite materials in space structures, new experiments were conducted to study the behavior of such materials under hypervelocity impact.[40] Besides the ground-based hypervelocity tests conducted by such entities as NASA MSFC, NASA JSC, and Air Force Research Lab, additional data were collected from the Long Duration Exposure Facility (LDEF) aboard a low-earth-orbiting satellite.

In the early 1990's, a group of researchers at the University of Toronto Institute for Aerospace Studies began compiling an extensive database of hypervelocity impact test results on polymeric composite materials. The database also includes the meteoroid / orbital debris impact data collected from the LDEF satellite.[41,42]

Lamontage et al.[43] performed a series of impact tests using light gas gun with 1-mm and 2-mm 2017 aluminum projectiles hitting the target plate at 5 km/s and at 0º, 30º, and 45º incidence angles. As target, they used 16- and 24-ply carbon/PEEK (AS4/APC-2) laminate specimens at 1.8 mm and 2.6 mm thickness, respectively, with symmetric quasi-isotropic lay-up of 0/±45/90 plies. The oblique impact angle is of particular interest as it can influence the debris cloud cone angle behind the shield. Their test results showed that the debris cloud exiting the target plate does not follow the line of flight of the projectile, and that the turning angle appears to be independent of the thickness of the plate but highly dependent on the impact angle. For a given impact energy, they found the damage area for the thicker 24-ply laminate to be nearly twice that in the 16-ply plate. Neither the number of plies in the laminate nor the impact angle was found to have any significant influence on the diameter of the entry crater. They conclude that since the target plate is thin relative to the projectile diameter, the hole size is influenced most by the impact velocity and the initial passage of the shock waves and not by the impact angle.

In the case of a double-wall design, however, as a result of an oblique impact with the bumper, the debris cloud angle does change, which in turn could result in reduced impact on the rear wall. Interestingly, Lamontage et al.[43] found that their 5 km/s impact-test data for carbon/PEEK can be closely modeled by Eq. (4) if the experimental data for measured hole diameter are scaled by a factor of 0.9 to account for the larger hole size in the composite target. As the authors also point out, there is no theoretical basis for this scale factor, and it is not clear if it will result in good agreement with other test data.

Extending the earlier study, Lamontage[44] investigated the impact response of carbon/PEEK target plates by examining the entry and exit crater diameters, the delamination damage areas in the front and back side of the target plate, and the debris cloud dispersion cone angle behind the

target. The parameters considered include the projectile impact velocity and angle, density, and diameter, as well as the thickness, ply orientation angle, and number of plies in the composite laminate. In addition, the effects of using a layer of ceramic fabric Nextel behind the primary shield and ahead of the aluminum witness plate were studied. The test results indicated that the Nextel layer is very effective in breaking up the impacting debris cloud behind the primary shield and preventing the ensuing particles that penetrated it to cause perforation, spalling, or cratering of the witness plate. The effectiveness of the Nextel layer is shown to increase as it is moved farther behind the front shield. The use of two layers of Nextel with one placed immediately behind the front shield did not show any significant improvement in reducing the impact damage to the front shield and those behind it.

3.1 Meteoroid Impact Shield Design

Inspired by the meteoroid and orbital debris protection system (MDPS) incorporated into the designs of ISS modules and nodes along with the hypervelocity impact test results reported in the literature, a double-bumper shield design is proposed for the MLH as shown in Fig. 6. For ease of manufacture, inspection, and repair or replacement, the meteoroid impact shielding (MIS) is made modular as is the case in the ISS.

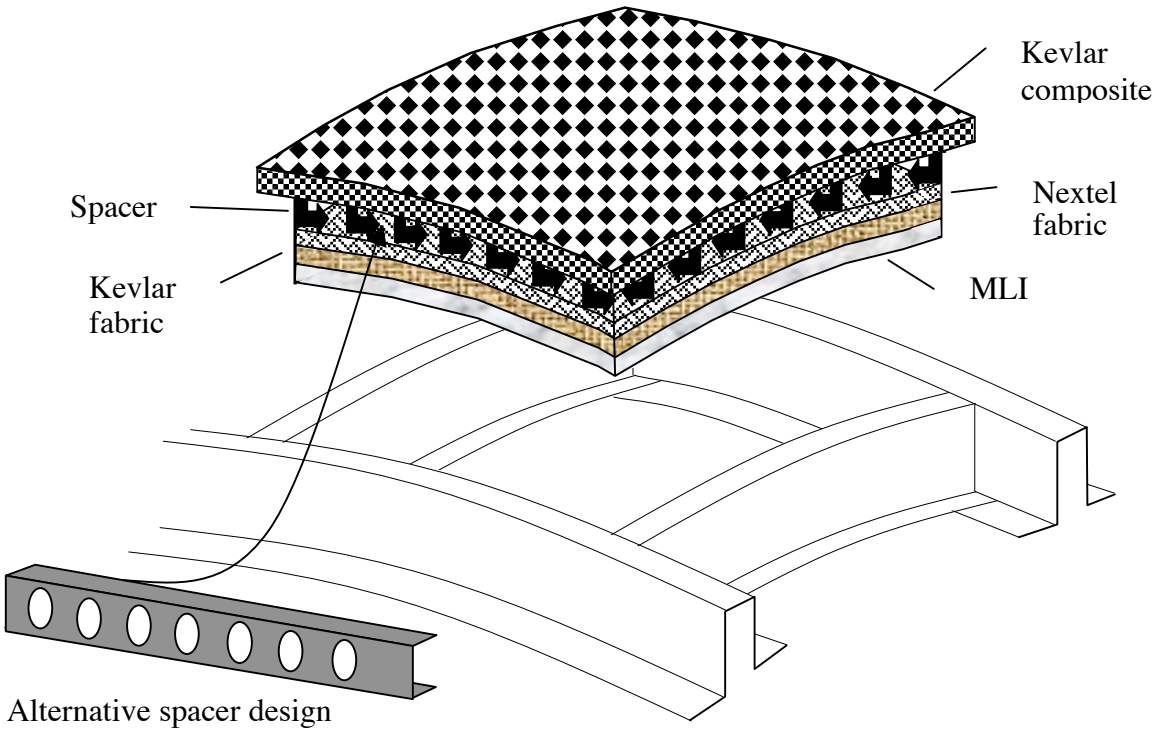

Figure 6: Composition of modular MIS panel (not to scale).

The front and rear bumpers are held at a fixed distance from each other with the help of C-spacers or a channel section having multiple holes (see Fig. 6) to allow the venting of trapped air during launch. The longerons and frames placed on the outside surface of the pressure vessel

wall, as shown in Fig. 6, will provide the base structure on which the MIS panels can be mounted.

Figure 6 also shows the proposed arrangement of the layering system for MIS. However, unlike the MDPS design on ISS modules, both front and rear bumpers are to be made of high-strength, impact-resistant advanced composite materials. The front bumper is to be made of Kevlar-reinforced polymer composite material (three-dimensional woven fabric) whereas the rear bumper is to be made of two tightly woven blankets of Nextel (primary layer) and Kevlar fibers that are stitched together by high-strength glass or polyethylene (Spectra) yarn. The stitching of the two blankets is expected to enhance the rear wall's damage tolerance and penetration resistance under hypervelocity meteoroid impact.

Ceramic Nextel®, aramid Kevlar®, and polyethylene Spectra® are all commercially available materials. In addition to increasing the impact resistance of MIS panels, the layer of Nextel will also enhance the passive thermal shielding of the habitat.

In absence of engineering analysis, no recommendation can be made at this time regarding the minimum thickness of the front or rear bumper. The same is also true about the spacing between the two bumpers and that between the rear bumper and the pressure-vessel wall. However, taking the ISS MDPS design as a guide, the Kevlar composite front bumper would have a minimum thickness of 0.25 cm (0.1 in). The Nextel and Kevlar layers would be approximately 0.30 cm (0.12 in) and 0.64 cm (0.25 in) thick, respectively, with the spacing between the front and rear bumper at approximately 10 cm (3.94 in) or preferably even greater if possible.

3.2 Texturing of Exposed Surfaces

Previous research indicates that oblique impacts above a critical angle are less damaging to the back wall than those at normal incidence.[45] With that in mind, the probability of oblique impact would greatly increase if the exposed surfaces of the habitat are covered by a textured blanket as shown in Fig. 7. The textured blanket represents an auxiliary, nonstructural layer to be placed atop the Kevlar composite front bumper. In addition to altering the impact angle, the pyramid design is expected to localize the damage zone to a smaller and possibly repairable area.

Because of the range of expected temperatures on the Moon, it is crucial for the textured layer to be made of a material that can retain sufficient elasticity / rigidity at both ends of the temperature spectrum.

Most ceramic-matrix composite materials such as carbon/carbon and carbon/silicon-carbide can tolerate the extreme high and low temperatures fairly well, but they tend to be rather brittle. There is some uncertainty about the performance of a ceramic shield under meteoroid impact at

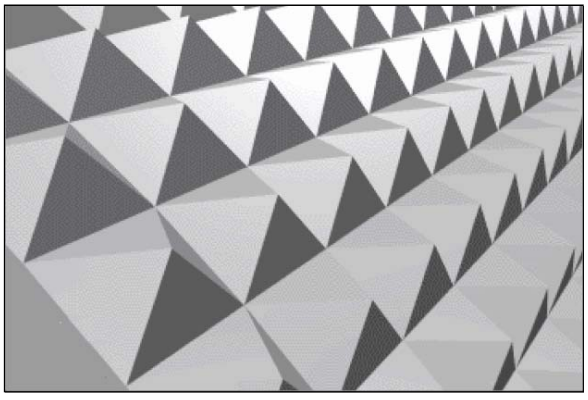

Figure 7: Pyramid texturing of exposed surfaces. (drawing by D. Dunn)

cryogenic temperatures. One concern is that upon impact, the ceramic layer may break into small pieces increasing the number of fragments in the debris cloud behind the first bumper.

Thermoplastic polymeric materials such as PEEK and polyimide, with the latter commonly used as the substrate material for thermal insulation blankets, may prove to be more appropriate for this application. In either case, the exposed surfaces will be coated to protect the material from deteriorating under prolonged exposure to ultraviolet light.

It is also not clear at this time whether the individual pyramid-shaped bumpers should be solid or hollow. If it is made hollow, then the air trapped inside could potentially act as an impact attenuator pushing parts of the debris fragments outward.

4. SHIELDING AGAINST EXTREME TEMPERATURES

In absence of any appreciable atmosphere, the ambient temperature near the lunar surface can fluctuate substantially from the sunlit to the shaded or dark areas. The lunar temperature in degrees Fahrenheit is expressed as[46]

$$T_M = (Cos\beta)^{0.25}\left((443 Sin\theta_s/\sigma)^{0.25} - 460\right) \quad (8)$$

where β is the Moon latitude (degrees), θ_s the solar-elevation angle (degrees), and σ the Stefan-Boltzman constant in units of Btu/(hr-ft^2-R^4). Depending upon the Moon latitude and solar elevation angle, the surface temperature can reach as high as +134ºC (273°F) and as low as -178ºC (-290°F).

Thermal radiation is the primary heat-transfer mechanism in free space. On the Moon, the sun and, to a lesser degree, the albedo from the sunlit lunar surfaces form the primary external heat sources.

The exterior walls of the MLH have to be designed such that the temperature inside the habitat is kept constant (near room temperature) while the outside temperature fluctuates drastically. Multi-layer insulation (MLI) blankets will be used as the primary thermal barrier although each MLH is expected to have an internal active heating and cooling system. The placing of MLI inside the MIS, as shown in Fig. 8, will protect it from being damaged by meteoroid impacts. In the actual design, the MLI blanket will cover the entire lower surface of MIS. However, for clarity, some portions of the MLI blanket are not shown in Fig. 8.

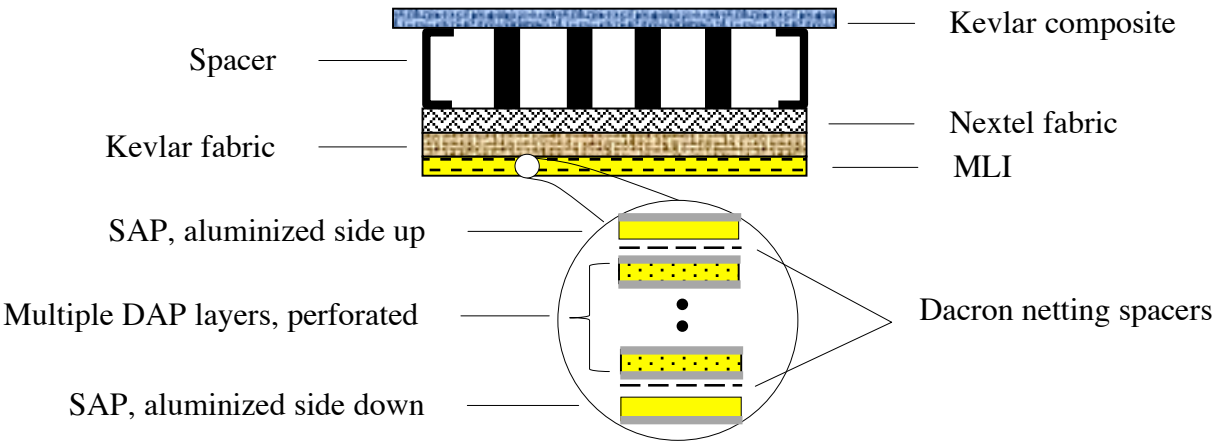

Figure 8: Placement and composition of MLI.

The heat radiated into or out of the MLH will depend on its surface reflectivity, emissivity, surface area, temperature, and geometric orientation relative to the heat source or sink. The surface finish and roughness influence the reflectivity and emissivity.

The MLI blanket will consist of multiple layers with low-emittance metallic coating on the polyimide or Fluoro ethylene propylene (FEP) substrate. In Fig. 8, the outer-most layers are shown to be single aluminized polyimide, SAP (e.g., Kapton) with the aluminum coated surfaces on the outside. The interior layers are made of double aluminized polyimide (DAP) to minimize heat transfer through them. The inner layers are also perforated to create an electrical connection between them to accommodate electrical grounding. The individual layers are separated by polyester or Dacron netting (spacer) to minimize conductive heat transfer between them. Therefore, the total heat flux through MLI layers is due to radiation, residual gas conduction, and solid spacer conduction.

Chorowski et al.[47] developed an optimization algorithm for finding the minimum number of layers in an MLI blanket based on the thermal properties of individual layers and the specified boundary temperatures. They considered radiation, solid spacer conduction, and residual gas conduction as the heat transfer modes. They calculate the total heat flux using an electrical network analogy with the three heat transfer modes treated as parallel thermal impedance between two adjacent layers. Their analytical predictions correlated well with experimental data. Among their findings, they show that at low residual gas pressures ($< 10^{-4}$ Pa), the gas conduction contribution to the total heat transfer flux is negligible. They also show that for a given number of layers, the total heat flux is greater for higher residual gas pressures. With the residual gas pressure set at 10^{-4} Pa, they show that the total heat flux increases with addition of more layers before reaching a plateau around $N_{Layers} = 17$, whereas at 10^{-3} Pa, the total heat flux decreases with addition of more layers without reaching a limit.

5. CONCEPTUAL DESIGN OF MLH

The proposed architecture for MLH, as shown in Fig. 9, is derived from the ISS US Lab module with a diameter (pressure vessel only) of 4.22 m (166 in) and length of 8.66 m (341 in). Its exterior dimensions are constrained by the interior dimensions and clearances of the single-manifest payload fairing of the Delta IV family of rockets. In addition to a hatch at each end, MLH is equipped with two lateral ports that are similar in size and shape to those on any of the ISS Nodes.

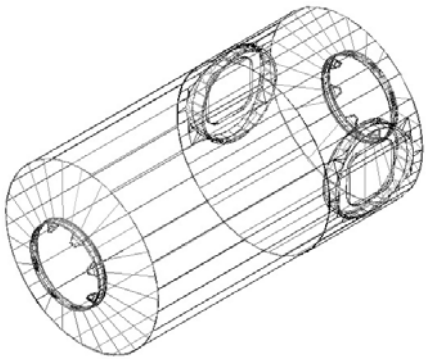

Figure 9: Conceptual model of MLH. (drawing by D. Dunn)

The inclusion of lateral ports is to accommodate connectivity with additional MLH units to form a larger lunar outpost. Three of many possible expansion configurations are shown in Fig. 10. The figure also shows an airlock for extravehicular activities.

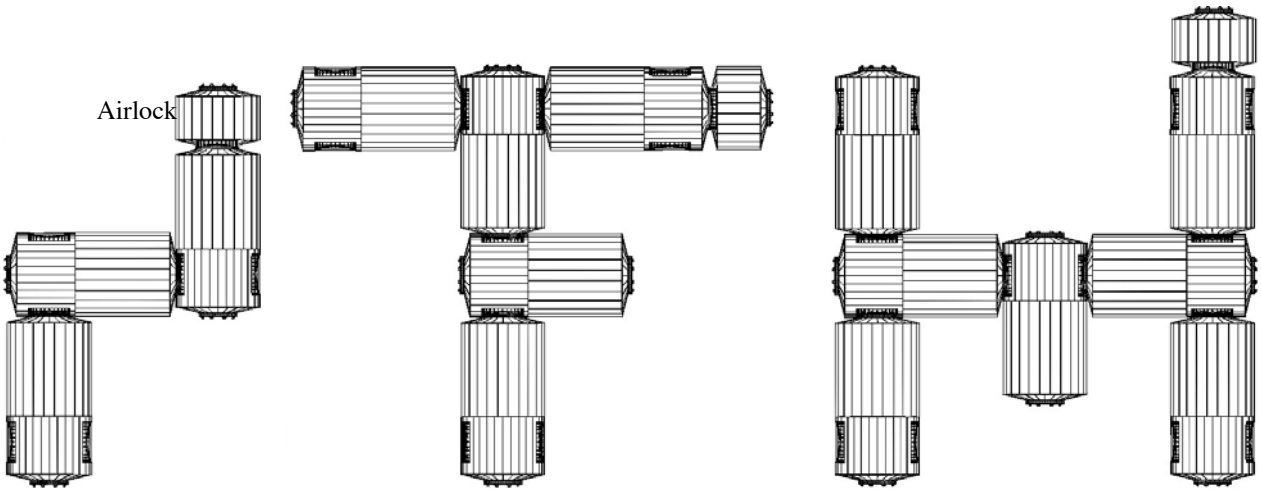

Figure 10: Three examples of docking options for an expanded lunar outpost.

The placement of side ports near one end is to make use of the existing support frame at the cylinder-cap transition section thereby reducing the structural weight of MLH. In addition, this placement provides larger uninterrupted wall sections for placement of equipment racks and various interior subsystems.

For greater mobility over the lunar terrain, MLH is equipped with six independently controlled articulated legs as shown in Fig.11. Each leg is powered by an electric motor at its base. Although the legs are designed to mainly accommodate motion in the longitudinal plane, the ball-and-socket support at each leg base also makes it possible for the MLH to move in the lateral direction for a total of three degrees of freedom.

The approach for launch, orbital transfer, descent, and landing is based on the concept proposed by Smitherman.[48] Each MLH descends and lands on the lunar surface with the help of two landing modules, one at each end, as shown in Fig.12. Upon landing, the legs of MLH will be extended and the landing modules will be detached. The landing modules are subsequently launched back to a stationary lunar orbit to be refueled and to bring additional MLH units down to the lunar surface.

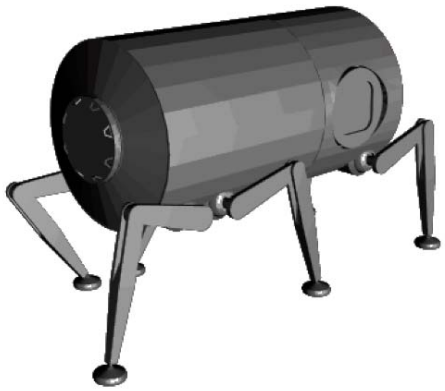

Figure 11: MLH with its articulated legs. (drawing by D. Dunn)

In lieu of large translucent windows that might compromise radiation and meteoroid impact shielding, the crew can have the view of the outside through closed-circuit video projected on to flat-panel displays. There could be up to 4 display panels, one on each side, used as virtual windows.

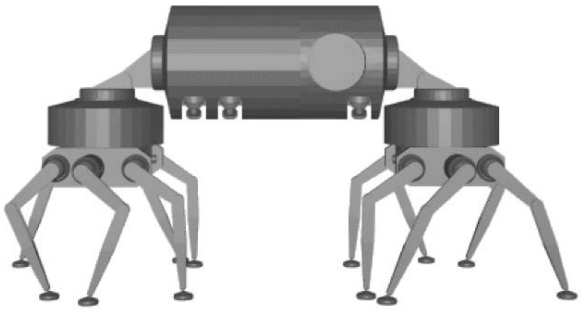

Figure 12: MLH with two landing modules. (drawing by D. Dunn)

The primary structure including the pressure vessel, internal and external frames and stiffeners, as well as the end hatches and side ports will all be made of carbon-reinforced polymer composite material. The proposed manufacturing process for individual parts and the overall assembly are discussed in the next section.

For radiation shielding, the entire pressure vessel shell will be sandwiched between two "thick" layers of polyethylene as shown in Fig. 13. The two polyethylene layers are assumed to have nearly the same thickness for a total of approximately 10 cm. In addition to shielding around the outer wall, the floor will be made of sandwich panels with polyethylene core. In a solar flare event, the available space beneath the floor panels can be used as TESS, Temporary Storm Shelter. While polyethylene will be the main radiation shielding material for the top and bottom surfaces of TESS, fresh and wastewater can be used for shielding the vertical walls.

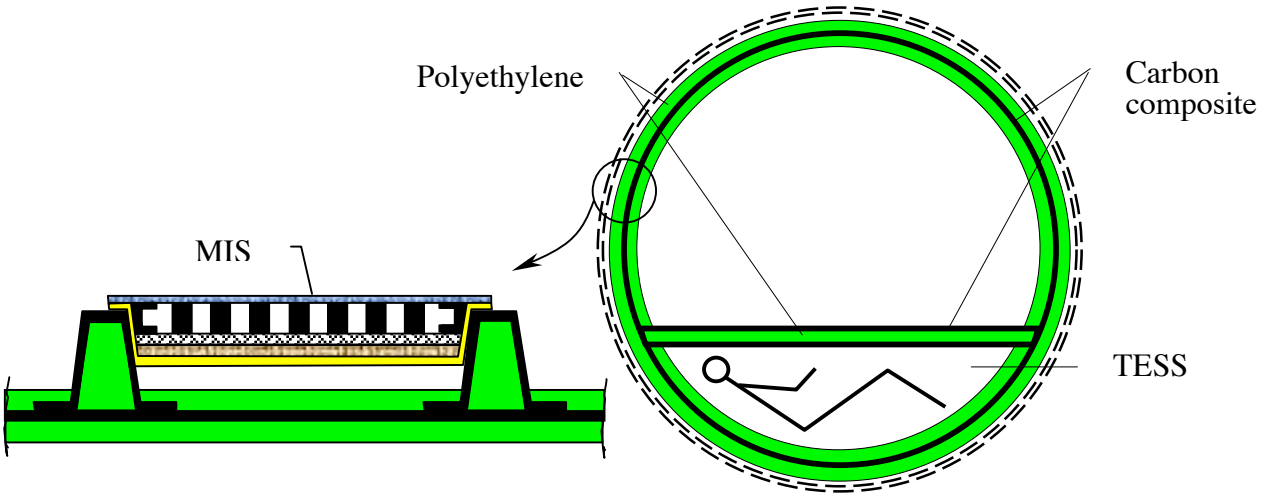

Figure 13: Cross-sectional views of the pressure vessel and its outer walls.

6. PROPOSED MANUFACTURING PROCESSES

The manufacturing process is dictated primarily by part size, geometric complexity, and material system. In the case of MLH, it is proposed to manufacture the structure as separate parts, all made of carbon-epoxy composite material, which are then assembled together to create the habitat structure. The structural parts include: the cylinder, end cones, lateral ports and end hatches, port and hatch frames, leg stowage boxes, external longerons and rings, internal support structure, and floor panels. Figure 14 shows the structural breakdown of MLH with the internal and external support structures omitted.

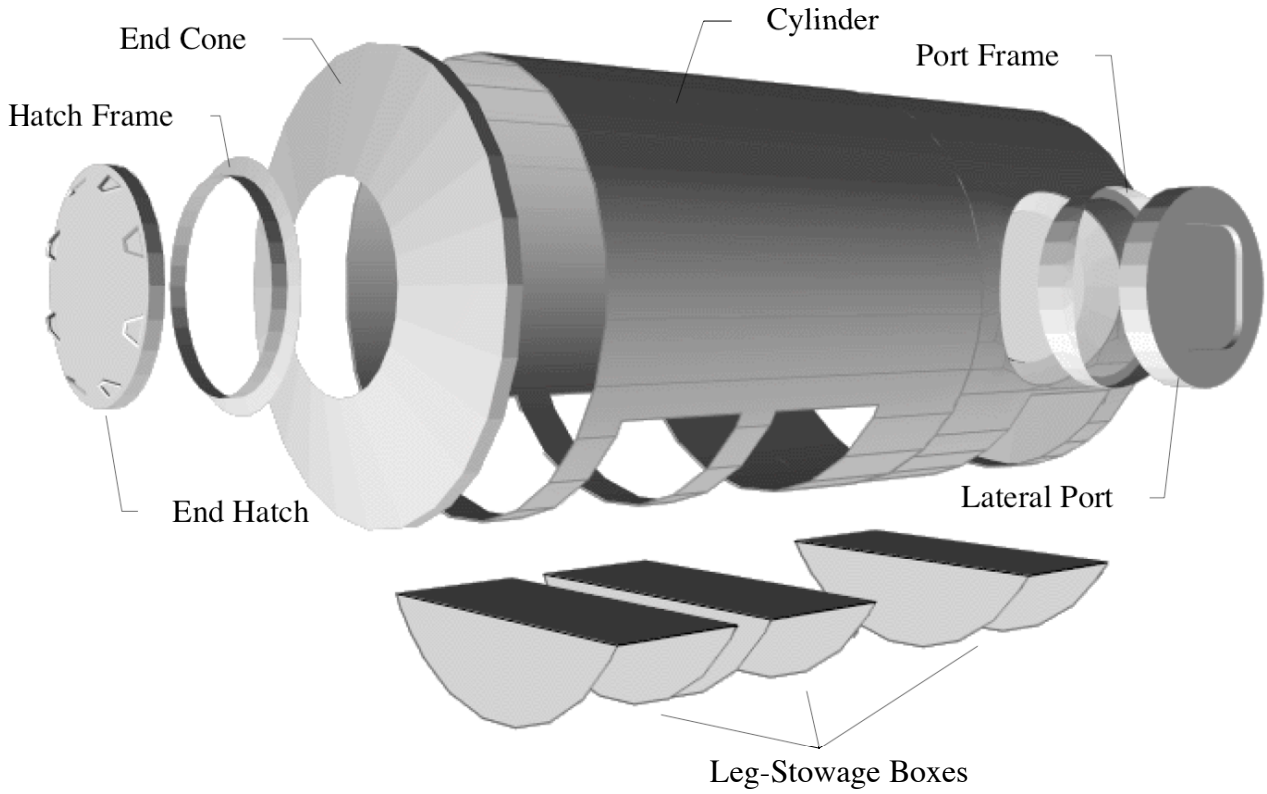

Figure 14: Breakdown of major structural parts. (drawing by D. Dunn)

For geometric stability and fabrication ease, all parts will have a symmetric lay-up with ply pattern resulting in a nearly quasi-isotropic laminate with no shear-extension or bending-extension coupling. The number of plies in each part will depend on the required strength and stiffness, and can vary from one part to another.

In this section, a brief description of the manufacturing process for each part is presented.

6.1 Main Cylinder

The cylindrical portion of the pressure vessel is to be fabricated using the filament-winding process as shown in Fig. 15. Typically, dry strands of reinforcement material are dipped into a pool of matrix material before getting wrapped around the axisymmetric mandrel. The carriage speed and the rotating speed of the mandrel determine the fiber direction. For a cylindrical pressure vessel, the bulk of the fibers should preferably be along the hoop and axial directions. Because of the carriage and mandrel setup, it is not possible to run the fibers along the axis, and typically the fiber direction is limited to angles greater than ±10° relative to the cylinder axis. Filament winding is an ideal process for the fabrication of composite cylinders. However, in the case MLH, size may be a problem.

Once the filament-winding process is completed, the part and the mandrel inside it are removed from the machine, and the thermoset matrix is allowed to fully cure before removing the part.

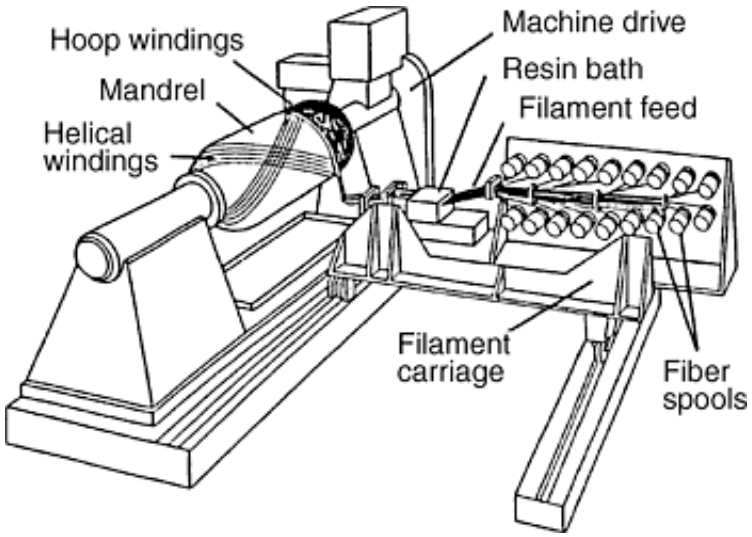

Figure 15: Filament winding machine. (figure from Ref. 49)

For advanced applications, carbon-composite parts are typically cured inside an autoclave based on specific variations in temperature and pressure during the cure cycle, which can last for up to 10 hours or more. For carbon-epoxy (e.g., AS4-3502) material, typical cure-cycle values for max temperature and pressure are 400°F and 350 psi, respectively. The elevated temperature enhances the irreversible chemical cross-linking of the thermoset material whereas the increased pressure improves the bonding of layered fibers and eliminates voids. For a pressure vessel of this kind, it is vital that the wall be nonporous to avoid oxygen leakage and pressure loss. If an appropriate-size autoclave is not available, then the cylinder would need to be vacuum bagged and kept under elevated temperature and vacuum till the thermoset matrix is fully cured. Because of reduced pressure, it is possible to have entrapped air bubbles causing some degradation in the part's structural characteristics.

Upon completion of the cure cycle, the end caps will be cut off and the cylindrical part removed from the mandrel. Moreover, the lateral-port and leg-stowage openings will be cut out as part of the manufacturing process. Depending upon the mandrel material, it is possible to reuse the mandrel for fabrication of additional cylinders.

6.2 End Cones

It is proposed to manufacture the end cones using the manual lay-up process. Layers of matrix-impregnated "prepreg" carbon fabric are cut to desired shapes and laid over a female mold, one at a time. The use of female mold will increase the dimensional accuracy of the outer surface. The end cone is flanged around its rim to facilitate its attachment to the inside wall of the cylinder. With all layers in place, the part is vacuum bagged and cured inside an autoclave.

Upon completion of the cure cycle and removal of the part from the mold, the outer edge will be trimmed and the opening for the hatch will be cut out.

6.3 Hatches and Ports

The complexity of these parts would require the use of vacuum-assisted resin transfer molding (VARTM) or its more advanced variant the SCRIMP process, as shown in Fig. 16. In the SCRIMP process, the individual layers of fabric are placed inside the mold in dry form and vacuum bagged before the injection of resin. Once resin injection is completed, the part is placed inside autoclave and cured.

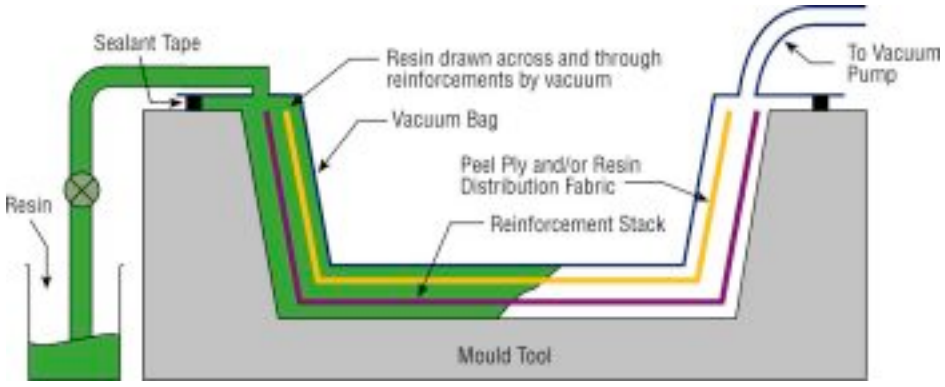

Figure 16: Graphical depiction of the SCRIMP process. (figure from Ref. 50)

6.4 Hatch and Port Frames

Compared to the hatches and ports, the supporting frames are much less complex. This will allow the frames to be manufactured using pre-preg fabrics and the manual lay-up process using female molds. Upon vacuum bagging the part, it is cured inside an autoclave.

6.5 Leg Stowage Boxes

With inside dimensions being critical, these parts will be made using male molds. As in the case of the end cones, the manual lay-up process will be used. The curved edges of each box will be flanged for attachment to the main cylinder. For additional stiffness, the two parallel walls will have several narrow composite planks inserted in the middle of the laminate.

6.6 External Longerons and Rings

External framing is needed to brace the pressure vessel during the launch-to-orbit phase of the flight and to provide a support structure for the attachment of MIS panels. Additionally, they are fitted with attachment points for connection to the payload-support structure of the launch vehicle.

One-dimensional parts, such as the longerons with hat-shape cross-section, are easily produced using the pultrusion process as shown in Fig. 17. These parts are dominated with axial loading and require the fibers to be placed predominantly along the axis.

The rings on the other hand are essentially curved beams and would require molded construction. It is possible to make the rings in one or two parts. The two-part construction will reduce the manufacturing complexity in the assembly process and would be the preferred route.

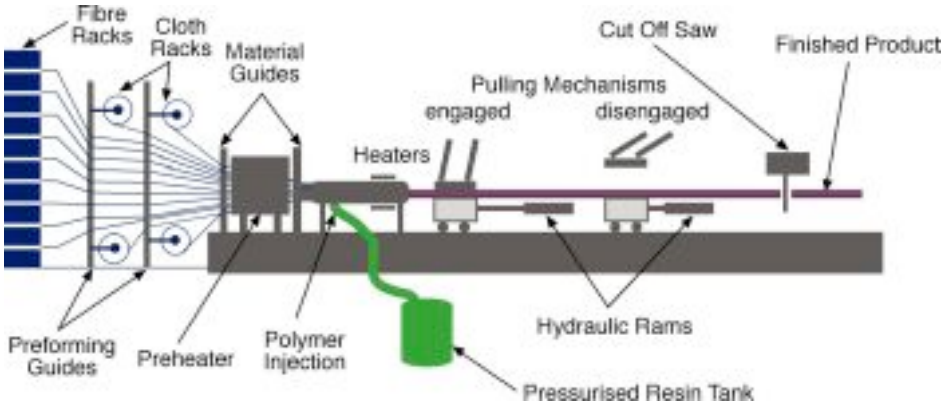

Figure 17: Graphical depiction of the pultrusion process. (figure from Ref. 50)

6.7 Internal Frame Structures

The internal framing will include three large frames to support the structure at critical sections, one at each cylinder-cone intersection and another near the side ports as shown in Fig. 18. The substructure beams for flooring and internal racks will be connected to these frames.

Whereas the beams can be made using the pultrusion process, the frames need to be made using the molded construction technique similar to that used for hatches and ports.

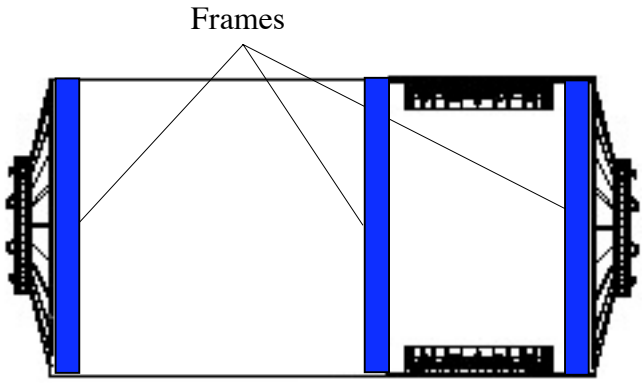

Figure 18: Internal frame locations.

6.8 Floor Panels

The floor panels will be of sandwich construction with carbon-epoxy face sheets and solid polyethylene core. Because of high temperature limitation of polyethylene, the face sheets will be fabricated separately and then adhesively bonded to the core.

6.9 Assembly

For composite structures of this type, the parts are typically bonded together with mechanical fasteners used only at specific locations.

7. PRELIMINARY STRUCTURAL ANALYSIS

Space structures encounter severe vibration and dynamic loads during launch and the initial flight phase. In most instances, these transient mechanical loads are more critical than the operational loads. However, in the absence of launch-specific loads data at this time, the internal pressure of 14.7 psi, as a representative operational loading condition, is used for the preliminary structural analysis.

The FE model, as shown in Fig. 19, was obtained by modifying a previously developed model of ISS US-Lab module. The major modification task involved the extension of its length and addition of two lateral ports. The design geometry of the lateral ports was taken from the ISS Node 1 model. The new model is 4.5 m (14.8 ft) in diameter and 9.3 m (30.5 ft) in length.

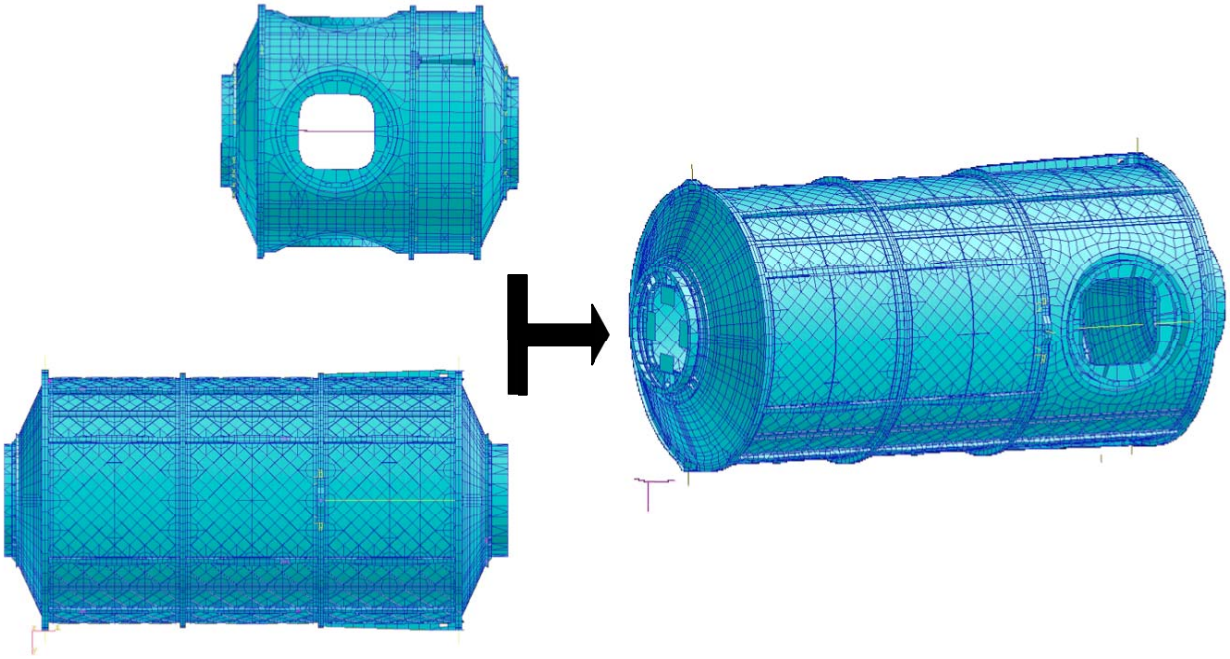

Figure 19: FE model of the MLH structure derived from ISS US-Lab and Node 1 models.

Such details as the internal framing or leg-stowage compartments were not captured in the FE model. Furthermore, no attempt was made to include any information related to MIS panels or polyethylene radiation shielding.

The initial focus of the analysis was to compare the structural weight of the baseline aluminum design with a hybrid design in which the cylinder portion, as shown in Fig. 20, is made of carbon-epoxy. For this analysis, the model of MLH without the lateral ports was analyzed using MSC/NASTRAN.

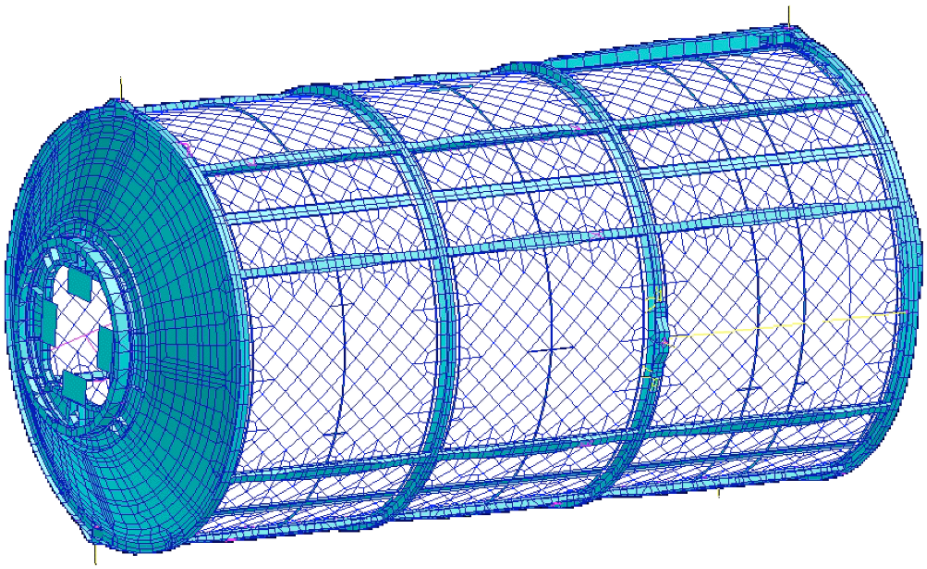

Figure 20: Analysis model with the cylinder wall shown in white.

For the baseline model with cylinder-wall thickness of 2.54 mm (0.1 in) and 2024-T3 material properties (see Table 2), the total strain energy under an internal pressure of 101.35 kPa (14.7 psi) was found to be 1.2546×10^4 N-m (1.1104×10^5 lb-in).

Table 2-a: Average properties for selected materials in SI units.

Material	Density, kg/m^3	Thermal conductivity, W/m-K	Specific heat, J/kg-K	Coeff. thermal expansion, 10^{-6}/C	Young's modulus, GPa	Poisson's ratio
Aluminum	2760	126	961	23.8	73.9	0.33
Carbon-epoxy[a]	1575	1.64	1020	17.4	46.2	0.34

[a] Quasi-isotropic properties at 60% fiber-volume fraction

Table 2-b: Average properties for selected materials in English units.

Material	Density, lb/in^3	Thermal conductivity, Btu/h-ft-F	Specific heat, Btu/lb-F	Coeff. thermal expansion, 10^{-6}/F	Young's modulus, 10^6 psi	Poisson's ratio
Aluminum	0.1	72.80	0.230	13.22	10.7	0.33
Carbon-epoxy[a]	0.057	0.95	0.244	9.67	6.7	0.34

[a] Quasi-isotropic properties at 60% fiber-volume fraction

The material in the cylinder portion was then changed to carbon-epoxy (see Table 2) and its thickness was adjusted until it had nearly the same strain energy (i.e., stiffness) as the baseline model. For a cylinder-wall thickness of 4.2 mm (0.165 in), the hybrid model was found to have a strain energy of 1.2431×10^4 N-m (1.1003×10^5 lb-in), which is about 1% less than that of the baseline model indicating a slightly stiffer model.

With the baseline and hybrid models having nearly the same stiffness, the weight comparison would be more meaningful. The structural weight for the baseline and hybrid models was found to be 7,632 kg (16,832 lb) and 7,452 kg (16,435 lb), respectively with the hybrid model being approximately 2.5% lighter.

The deflection contour plots of the baseline and hybrid models are shown in Fig. 21. In both cases, the maximum deflection was found to be approximately 7.11 mm (0.28 in).

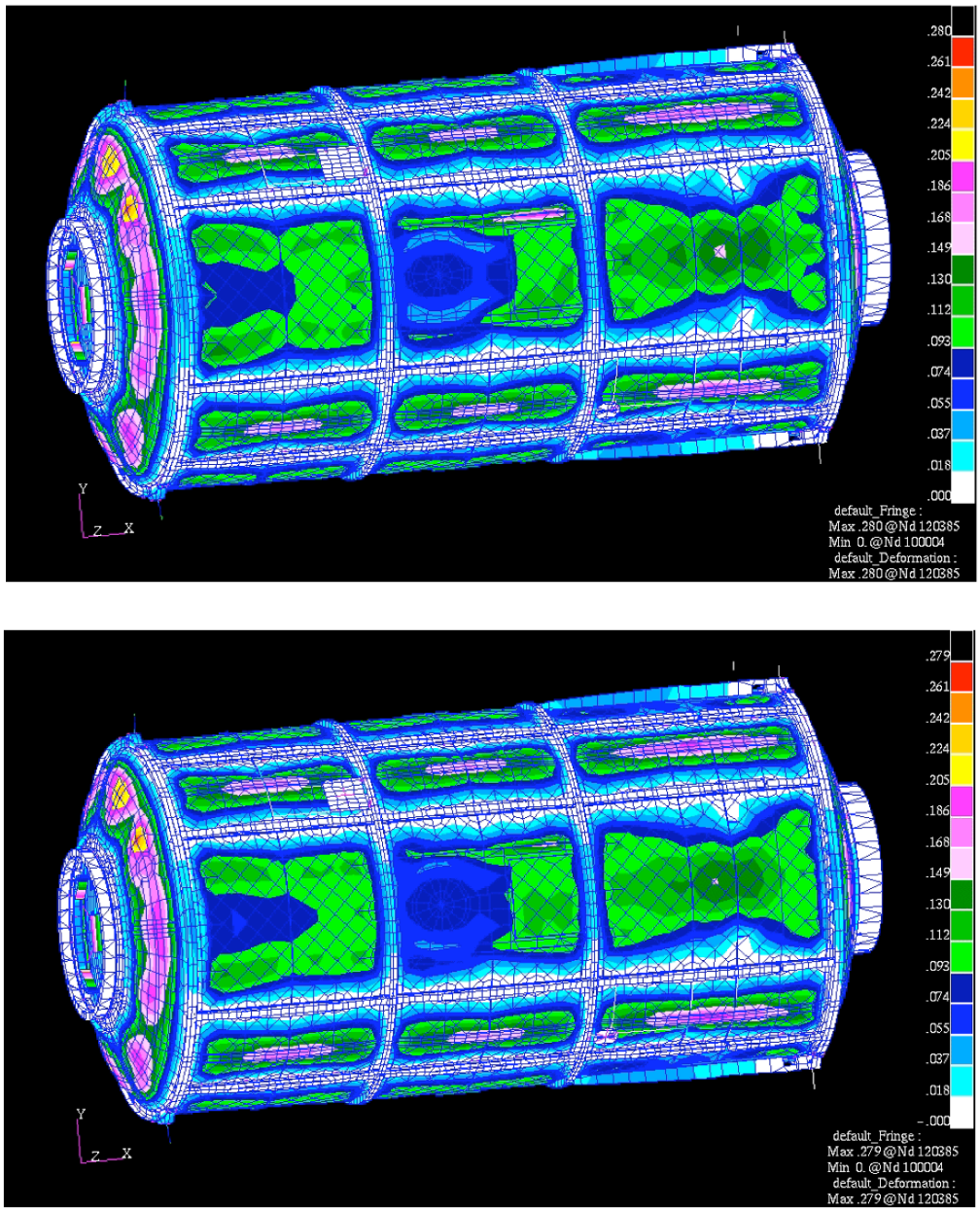

Figure 21: Deflection contour plots of the baseline (top) and hybrid models.

8. RECOMMENDATIONS FOR FUTURE WORK

The multi-disciplinary set of requirements makes the environmental shielding of the lunar habitat a systems design problem. However, as it became apparent in this research, there is still considerable uncertainty in several key areas—most notably meteoroid impact and radiation—requiring further research.

For example, the performance of the proposed double-wall composite MIS panels under hypervelocity impact requires both analytical and experimental verification. On the analytical side, it is recommended to use such hydrodynamic codes as PAM-SHOCK or AUTODYN to investigate the penetration resistance of MIS panels to various combinations of projectile speed and impact angles. Furthermore, the use of the optional textured blanket as the outermost layer of MIS needs to be investigated to determine whether it will in fact reduce or unintentionally increase the projectile impact damage. Both solid and hollow configurations together with alternative material systems need to be examined.

To verify the analytical impact penetration predictions, it is recommended to physically test several full-scale MIS panels. The projectile testing facilities such as those at the NASA JSC or the Southwest Research Institute in San Antonio, TX will have to be used for such experiments. Among the factors that need to be experimentally verified is the effect of panel temperature on the impact response.

Besides the geometric shape of MLH and the material system of its outer walls, the material composition and placement of its internal equipment can have a large influence on the radiation environment inside the habitat. It is recommended to use a computational tool such as SHIELDOSE to estimate the delivered dose inside the MLH with different shielding material systems and habitat configurations.

Besides the recommendations above, it is suggested to investigate the feasibility of a lunar mission with the goal of detail surveying of the hardware left behind during the Apollo missions for environmental damage. Details of the proposed mission are given in the Appendix. A major objective would be to determine the extent of damage caused by meteoroid impacts over the span of 35 years.

Similar to the LDEF used to collect information on material response to space environment in LEO, it is recommended to plan a mission thereby an LDEF-like experiment station can be established on the Moon. Potentially, the experiment station can consist of various shielded compartments inside which radiation dose can be measured and relayed back to earth. However, the exact details of such an experimental set up will need to be determined by experts in nuclear physics and radiation field.

Since the carbon-composite pressure vessel is to be covered by multi-layered insulation, it is expected to operate at temperatures that would not approach anywhere near the extreme temperatures outside of MIS panels. However, such design details as the sizing of structural

elements, choice of candidate material systems, attachment of internal and external stiffeners to the pressure-vessel wall, and the installment of MIS panels need further investigation.

As a system engineering problem, the MLH as a whole and its environmental shielding in particular, would be ideal candidates for application of multi-disciplinary design optimization (MDO) methodology. By establishing proper links between various analysis tools for structural response and environmental effects assessment in combination with a design optimization tool within an MDO framework, it would be possible to conduct a detailed design sensitivity analysis and to optimize the MLH design to minimize its weight or cost while maintaining the desired habitat characteristics.

Many design details were not addressed in this research. For example, the support structure for the legs and the structural cut-outs to accommodate their stowage in transition to the Moon have not been analyzed. By establishing the proper sizing of the legs and their power requirement, additional engineering analysis can be conducted to determine among other things the loads that they would exert on the main MLH structure. Details related to the leg-stowage boxes will also require further analysis. Although internal pressure is the primary operational load, the resulting stresses are expected to be significantly less than those encountered during launch. It is necessary, therefore, to size the structural elements based on the extreme loads encountered in the initial phase of flight-to-orbit. This would require better understanding of the launch scenario and the induced vibration and dynamic loads.

The manufacturing processes suggested in this report need to be examined further once additional structural details are available. For example the use of the filament-winding process and the subsequent curing of the composite part inside an autoclave could be a problem. If indeed, it is not possible to cure the large cylinder inside an autoclave, then it will be necessary to build similar components under less ideal conditions and test the performance of the resulting structure.

At the Raspet Flight Research Laboratory (RFRL) in Mississippi State University, we have a large prototype composite structure manufacturing facility that includes an Arboga 5-axis CNC milling machine with a18 ft x 14 ft x 3 ft cutting table along with three autoclaves ranging in interior size from 2 ft x 4 ft up to 10 ft x 55 ft. Autoclave pressures range from 100 psi up to 300 psi and curing temperatures range from 350 up to 850ºF. Besides the computational design expertise, we have the ability to build large scale components using prepreg carbon-epoxy or other similar composite materials. It is recommended to use the RFRL facilities to design and build a scaled version of MLH (or a section of the full-size model) as a technology demonstrator and as a test bed for assessment of the mobility system, MIS integration, and the overall design architecture. This activity can supplement related work at the NASA MSFC.

REFERENCES

1. Kokh, P., "Using Lavatubes for Shelter on the Moon and Mars," http://www.Lunar-reclamation.org/habitatmoonmars_2.html.
2. Nagem, R., Bon, R., Sandri, G., and Weaver, M.K., "Pneumatic Structures for Lunar and Martian Habitats," Building Research and Information, Vol. 19, No. 1, pp. 43-49, 1991.
3. Yin, P.K., "Structural Design of an Inflatable Lunar Habitat," Proceedings of Space 90 April 22-26, 1990, volume 1, 1990, p 520-528.
4. Sture, S., Jolly, S.D., and Happel, J., "A Near-Term, Long-Duration, Lunar Outpost Design," Proceedings of the 4th International Conference on Engineering, Construction, and Operations in Space, 1994.
5. Day, J. and Richter, P., "Analysis of Lunar Membrane Structures for Potential Failure Scenarios," Proceedings of the International Conference on Engineering, Construction, and Operations in Space, Vol. 2, 1996, p 1052-1058.
6. Schwartz, M. and Leonard, R. S., "Innovative Radiation Shields for Lunar Surface Operations," Proceedings of the International Conference on Engineering, Construction and Operations in Space, 1996.
7. Dorrity, J.L. and Brazell, J.W., "Constructing Radiation Shields with Textiles for Lunar Applications," Proceedings of the 3rd International conference on Engineering, Construction, and operations in space, 1992.
8. NASA, http://www.jsc.nasa.gov/er/she/gotomoon.html.
9. Drake, R.M. and Richter, P.J., "Concept Evaluation Methodology for Extraterrestrial Habitats," Journal of Aerospace Engineering, Vol. 5, No. 3, July 1992.
10. Mankins, J., "Modular Architecture Options for Lunar Exploration and Development," Space Technology, Vol. 21, No. 1-2, pp. 53-64, 2001.
11. Cohen, M. M., "Mobile Lunar and Planetary Bases," Proceedings of Space 2003 Conference, Long Beach, CA, April 23-25, 2003, AIAA-2003-6280.
12. Simonson, L.C. and Nealy, J.E., "Radiation Protection for Human Missions to the Moon and Mars," NASA TP-3079, 1991.
13. Shea, M.A. and Smart, D.F., "A Summary of Major Solar Proton Events," Journal of Solar Physics, Vol. 127, pp. 297-320, June 1990.
14. Parnell, T.A., Watts, J.W., and Armstrong, T.W., "Radiation Effects and Protection for Moon and Mars Missions," Proceedings of the 6th International Conference on Engineering, Construction, and Operations in Space, 1998.
15. Wilson, J.W., Cucinotta, F.A., Miller, J., Shinn, J.L., Thiebaeault, S.A., Singleterry, R.C., Simonson, L.C., and Kim, M.H., "Materials for Shielding Astronauts from the Hazards of Space Radiations," Material Research Society Fall Meeting, Boston, MA, Nov. 30 – Dec. 4, 1998.
16. National Council on Radiation Protection and Measurements, "Guidance on Radiation Received in Space Activities," NCRP Report No. 98, July 31, 1989.
17. 1990 Recommendations of the International Commission on Radiological Protection. ICRP Publication 60, Pergamon Press, Inc., 1991.
18. Kim, M.Y., Wilson, J.W., Thibeault, S.A., Nealy, J.E., Badavi, F.F., and Kiefer, R.L., "Performance Study of Galactic Cosmic Ray Shield Materials," NASA TP-3473, 1994.
19. Bertell, R., No Immediate Danger?: Prognosis for a Radioactive Earth, The Book Publishing Company, 1995.
20. Denkins, P., Badhwar, G., Obot, V., Wilson, B., and Jejelewo, O., "Radiation Transport Modeling and Assessment to Better Predict Radiation Exposure, Dose, and Toxicological Effects to Human Organs on Long Duration Space Flights," Acta Astronautica, Vol. 49, No. 3-10, pp. 313-319, 2001.
21. Wilson, J.W., Simonson, L.C., Shinn, J.L., Dubey, R.R., Jordan, W., and Kim, M., "Radiation Analysis for the Human Lunar Return Mission," NASA TP-3662, 1997.
22. Wilson, J.W., Chun, S.Y., Badavi, F.F., Townsend, L.W., and Lamkin, S.L., "HZETRN: A Heavy Ion/Nucleon Transport Code for Space Radiations," NASA TP-3146, 1991.
23. NOVICE software, Experimental and Mathematical Physics Consultants, Gaithersburg, MD.
24. Seltzer, S.M., "Updated Calculations for Routine Space-Shielding Radiation Dose Estimates: SHIELDOSE-2," NISTIR 5477, December 1994.
25. Cohen, M.M., "Carbon Radiation Shielding for the Habot Mobile Lunar Base," 34th International Conference on Environmental Systems (ICES), Colorado Springs, CO., July 19-22, 2004.

26. Wilson, J.W., Cucinotta, F.A., Simonson, L.C., Shinn, J.L., Thibeault, S.A., and Kim, M.Y., "Galactic and Solar Cosmic Ray Shielding in Deep Space," NASA TP-3682, 1997.
27. Townsend, L.W., Nealy, J.E., Wilson, J.W., and Simonson, L.C., "Estimates of Galactic Cosmic Ray Shielding Requirements During Solar Minimum," NASA TM-4167, 1990.
28. Singleterry, R.C. and Thibeault, S.A., "Materials for Low-Energy Neutron Radiation Shielding," NASA TP-2000-210281, 2000.
29. Landis, G.A., "Magnetic Radiation Shielding: An Idea Whose Time Has Returned?," Presented at the 10th Biennial SSI/Princeton Conference on Space Manufacturing, Princeton, N.J., May 15-19, 1991.
30. Anderson, J., Environments Group, Engineering Systems Department, NASA Marshall Space Flight Center, Personal communications, June 2004.
31. Anderson, J. and Smith, R.E., "Natural Orbital Environment Guidelines for Use in Aerospace Vehicle Development," NASA TM-4527, 1994.
32. Nikolova, S. and Jones, J., "Lifetimes of Meteoroids in Interplanetary Space: The Effect of Erosive Collisions and Planetary Perturbations," Proceedings of the Meteoroids 2001 Conference, Swedish Institute of Space Physics, Kiruna, Sweden, August 6-10, 2001.
33. Cour-Palais, B.G., "Meteoroid Environment Model – 1969 [Near Earth to Lunar Surface]," NASA SP-8013, 1969.
34. Hayashida, K.B. and Robinson, J.H., "Double-Plate Penetration Equations," NASA TM-2000-209907, 2000.
35. Whipple, F.L., "Meteoroids and Space Travel," The Astronomical Journal, Vol. 52, No. 1161, p.131, 1947.
36. Hayashida, K.B. and Robinson, J.H., "Single Wall Penetration Equations," NASA TM-103565, 1991.
37. Gardner, D.J., McDonnell, A.M., and Collier, I., "Hole Growth Characterisation for Hypervelocity Impacts in Thin Targets," International Journal of Impact Engineering, Vol. 19, No.7, pp. 589-602, 1997.
38. PAM-SHOCK, Commercial Software, ESI Group, Paris, France.
39. AUTODYN, Commercial Software, Century Dynamics, Concord, CA.
40. Yew, C.H. and Kendrick, R.B., "A Study of Damage in Composite Panels Produced by Hypervelocity Impact," International Journal of Impact Engineering, Vol. 5, pp. 729-738, 1987.
41. Tennyson, R.C., "Composite Materials in Space – Results from the LDEF Satellite," Canadian Aeronautics and Space Journal, Vol. 37, No. 3, pp. 120-133, 1991.
42. Tennyson, R.C. and Manuelpillai, G., "Analysis of LDEF Micrometeoroid/Debris Data and Damage to Composite Materials," Proceedings of the Second LDEF Post-Retrieval Symposium, NASA CP-3194, pp. 493-511, June 1992.
43. Lamontage, C.G., Manuelpillai, G.N., Taylor, E.A., and Tennyson, R.C., "Normal and Oblique Hypervelocity Impacts on Carbon Fibre/Peek Composites," International Journal of Impact Engineering, Vol. 23, pp. 519-532, 1999.
44. Lamontage, C.G., "Hypervelocity Impact Damage to Polymer Matrix Composite Structures in Space," Ph.D. Thesis, Department of Aerospace Science and Engineering, University of Toronto, 2003.
45. Schonberg, W.P. and Taylor, R.A., "Penetration and Ricochet Phenomena in Oblique Hypervelocity Impact," AIAA Journal, Vol. 27, No. 5, pp. 639-646, May 1989.
46. Creel, R.A., "Applying Thermal Control Experience on Apollo Lunar Rover Project to Rovers for the Space Exploration Initiative," Space Frontier Foundation's Return to the Moon V Conference, Las Vegas, Nevada, July 16 – 18, 2004.
47. Chorowski, M., Grzegory, P., Parante, Cl., and Riddone, G., "Optimisation of Multilayer Insulation – An Engineering Approach," 6th IIR International Conference "Cryogenics 2000", Praha, Czech Republic, October 10-13, 2000.
48. Smitherman, D.V. ,Jr., Technical Manager, Advanced Projects Office, NASA Marshall Space Flight Center, Personal Communications, June 2004.
49. ASM Handbook, Vol. 21, Composites, 2001.
50. Netcomposites, http://www.netcomposites.com, 2004.

APPENDIX: LUNAR HARDWARE SURVEY AND RECOVERY MISSION

The Apollo missions were extremely useful in bringing back lunar rock and soil samples for detailed scientific studies on Earth. They also helped increase our understanding of the challenges and benefits of working and conducting scientific experiments in a low-gravity environment. However, there is an extremely important body of information from the Apollo missions that remains untapped and that is the environmental effects of prolonged lunar exposure on man-made materials and hardware.

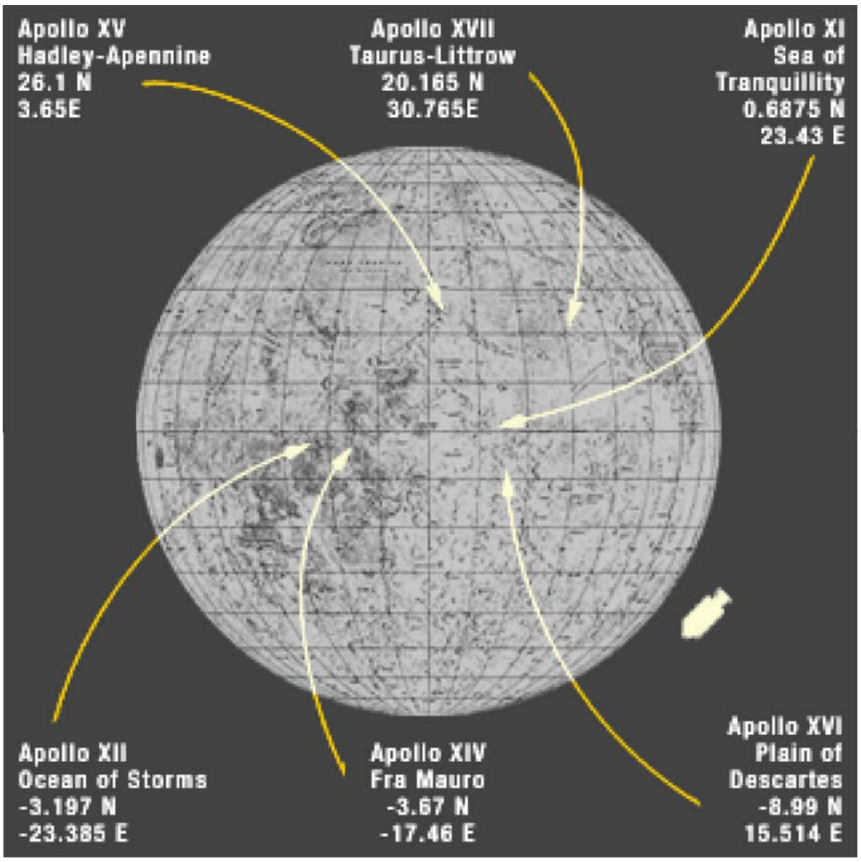

Source: http://spaceflight.nasa.gov/history/apollo/lunarlanding.html

From 1969 to 1972, there were a total of six successful human lunar missions. A different landing site was chosen for each mission as shown in the figure. Each mission left behind a myriad of hardware ranging from the descent section of the Lunar Module, to Lunar Roving Vehicle (LRV), and scientific equipment, some of which have been exposed to the lunar environment for 35 years.

Many important scientific and engineering questions can be answered through one or more robotic missions to some of the previous Apollo landing sites. Possible mission scenarios could include the following:

- Landing of a Surveying and Retrieving Robot (SRR) to perform
  - Visual inspection of hardware for visible signs of environmental damage including those caused by meteoroid impacts.
  - X-raying of hidden or otherwise sealed sites.
  - Retrieval of small and removal of samples from larger hardware to be brought back to Earth for detailed testing and evaluation.
  - Retrieval of environmental monitoring equipment left behind.

- Placement of an experiment station similar to LDEF to measure the effects of the lunar environment on samples of advanced composite materials that could be used as the construction material for future modular lunar habitats.

Some of the questions that such a robotic mission can help answer include:

- What is the meteoroid impact history on a large-size hardware at a specific lunar location?
- What is the extent of environmental damage to the hardware?
- What is the impact of prolonged radiation exposure on mechanical properties of structural materials and thermal properties of insulating materials?

NASA and others have developed several transport codes to compute the absorbed dose through various shielding materials or to simulate the effect of radiation on material properties. However, the computational predictions for HZE fluence have not been validated with data from experiments that closely mimic the extreme nature of the lunar environment. By evaluating the samples taken from the retrieved lunar hardware, we can gain better understanding of the lunar environment and its influence on materials.

Similarly, there is uncertainty about the threat posed by micrometeoroids and meteoroids. The Moon is believed to be regularly impacted by meteoroids at speeds of up to 72 km/s, but the meteoroid and lunar debris protection shield experiments conducted on Earth have not yet been able to exceed the limit of 11 km/s. Therefore, there is no experimental data that could be used to validate the results obtained from simulation codes that are likely to be used in design of future lunar habitats. Furthermore, a close survey of a hardware that was left exposed for more than three decades will give us more information about the severity of the threat.

To reduce the cost of the proposed robotic missions, many factors have to be considered, including the magnitude and diversity of hardware associated with each of the previous lunar landing missions as well as the geographic diversity of the landing sites. As shown in the figure, four of the Apollo landing sites were near the lunar equator with the remaining two at higher (i.e., > 20ºN) latitudes. Apollo 12 and 15 sites represent two candidate locations for the proposed retrieval mission considering both spatial extremes and diversity of hardware. For instance, Apollo 12 mission included the placement of Surface Experiments Package (ALSEP) whereas Apollo 15 mission included the use of the first LRV.

REPORT DOCUMENTATION PAGE

Form Approved
OMB No. 0704-0188

1. AGENCY USE ONLY *(Leave Blank)*	2. REPORT DATE	3. REPORT TYPE AND DATES COVERED
	April 2005	Contractor Report

4. TITLE AND SUBTITLE
On Structural Design of a Mobile Lunar Habitat With Multi-Layered Environmental Shielding

5. FUNDING NUMBERS
NNM04AA08G

6. AUTHORS
M. Rais-Rohani

7. PERFORMING ORGANIZATION NAME(S) AND ADDRESS(ES)
Mississippi State University
Mississippi State, MS 39762

8. PERFORMING ORGANIZATION REPORT NUMBER
M–1135

9. SPONSORING/MONITORING AGENCY NAME(S) AND ADDRESS(ES)
NASA Faculty Fellowship Program
George C. Marshall Space Flight Center
Marshall Space Flight Center, AL 35812

10. SPONSORING/MONITORING AGENCY REPO NUMBER
NASA/CR—2005–213845

11. SUPPLEMENTARY NOTES
Prepared for NASA's Faculty Fellowship Program by Mississippi State University
Technical Monitor: J.R. Pruitt

12a. DISTRIBUTION/AVAILABILITY STATEMENT
Unclassified-Unlimited
Subject Category 18
Availability: NASA CASI 301–621–0390

12b. DISTRIBUTION CODE

13. ABSTRACT *(Maximum 200 words)*

This report presents an overview of a Mobile Lunar Habitat (MLH) structural design consisting of advanced composite materials. The habitat design is derived from the cylindrical-shaped U.S. Lab module aboard the *International Space Station* (*ISS*) and includes two lateral ports and a hatch at each end that geometrically match those of the *ISS* Nodes. Thus, several MLH units can be connected together to form a larger lunar outpost of various architectures. For enhanced mobility over the lunar terrain, the MLH uses six articulated insect-like robotic, retractable legs enabling the habitat to fit aboard a launch vehicle. The carbon-composite shell is sandwiched between two layers of hydrogen-rich polyethylene for enhanced radiation shielding. The pressure vessel is covered by modular double-wall panels for meteoroid impact shielding supported by externally mounted stiffeners. The habitat's structure is an assembly of multiple parts manufactured separately and bonded together. Based on the geometric complexity of a part and its material system, an appropriate fabrication process is proposed.

14. SUBJECT TERMS
mobile lunar habitat, structural design/analysis, multi-layered environmental shielding, meteoroid impact shielding, habitat mobility

15. NUMBER OF PAGES
44

16. PRICE CODE

17. SECURITY CLASSIFICATION OF REPORT	18. SECURITY CLASSIFICATION OF THIS PAGE	19. SECURITY CLASSIFICATION OF ABSTRACT	20. LIMITATION OF ABSTRACT
Unclassified	Unclassified	Unclassified	Unlimited

National Aeronautics and
Space Administration
IS04
George C. Marshall Space Flight Center
Marshall Space Flight Center, Alabama
35812